Noninvasive Metabolic Monitoring:

An Assessment of Thermoelectric Gas Adsorption Biosensors

for Acetone and Ethanol Detection in Breath Analysis.

by

Kimberly Wilson

A Thesis Presented in Partial Fulfillment
of the Requirements for the Degree
Master of Science

Approved April 2011 by the
Graduate Supervisory Committee:

Eric Guilbeau, Co-Chair
Vincent Pizziconi, Co-Chair
Jeffrey LaBelle

ARIZONA STATE UNIVERSITY

May 2011

ABSTRACT

In the search for chemical biosensors designed for patient-based physiological applications, non-invasive diagnostic approaches continue to have value. The work described in this thesis builds upon previous breath analysis studies. In particular, it seeks to assess the adsorptive mechanisms active in both acetone and ethanol biosensors designed for breath analysis. The thermoelectric biosensors under investigation were constructed using a thermopile for transduction and four different materials for biorecognition. The analytes, acetone and ethanol, were evaluated under dry-air and humidified-air conditions. The biosensor response to acetone concentration was found to be both repeatable and linear, while the sensor response to ethanol presence was also found to be repeatable. The different biorecognition materials produced discernible thermoelectric responses that were characteristic for each analyte. The sensor output data is presented in this report. Additionally, the results were evaluated against a mathematical model for further analysis. Ultimately, a thermoelectric biosensor based upon adsorption chemistry was developed and characterized. Additional work is needed to characterize the physicochemical action mechanism.

In honor of Mr. & Mrs. Tucker and Mr. & Mrs. Wilson

ACKNOWLEDGEMENTS

Acknowledging those who have continued to support me throughout this process, I declare my eternal gratitude and appreciation. Thank you for your constancy and generosity.

TABLE OF CONTENTS

Page

TABLE OF CONTENTS iv

LIST OF TABLES vi

LIST OF FIGURES vii

LIST OF SYMBOLS ix

CHAPTER 1

1 INTRODUCTION 1

Noninvasive Sensing 1

Experimental Purpose 3

Review of Biosensor Device 3

Transduction via Thermoelectricity 4

Biorecognition via Heat of Adsorption 4

Clinical Significance of Biosensor Device 6

2 BACKGROUND and THEORY 9

Adsorption Fundamentals 9

Types of Adsorption 10

Theoretical Foundations for Describing Adsorption 12

Thermodynamic Principles for Describing Adsorption 17

Thermoelectric Phenomenon and the Thermopile 20

Theoretical Model for Biosensor Device 23

3 EXPERIMENTAL METHODS 29

Thermopile and Biosensor Fabrication 29

Biosensor Testing 30

Data Anlaysis 32

4 RESULTS 34

Transducer and Sensor Characterization 34

Chapter Page
Biorecognition Material Evaluation 35
Performance with Activated Charcoal 37
Performance with Semi-solid Polydimethylsiloxane 38
Performance with Solid Polydimethylsiloxane 40
Perfomance with Semi-solid Polytetrafluoroethylene 42
Theoretical Model Validation 43
5 DISCUSSION 46
Transducer and Sensor Characterization 46
Biorecognition Material Evaluation 46
Evaluation of Theoretical Model 50
6 CONCLUSIONS and RECOMMENDATIONS 52
REFERENCES 55
APPENDIX 58
BIOGRAPHICAL SKETCH 59

LIST OF TABLES

Table Page

2.1 Summary of thermoelectric applications using thermopiles. 24

5.1 Summary of data for both acetone and ethanol testing. 48

LIST OF FIGURES

Figure Page

2.1 Relationship between chemical adsorption and temperature (Sharma and Singh, 2011). 11

2.2 Relationship between physical adsorption and temperature (Sharma and Singh, 2011). 11

2.3 Sample isotherm generated from Langmuir theory (Sharma and Singh, 2011). 15

2.4 Sample isotherm generated from BET theory (Sharma and Singh, 2011). 17

2.5 Energy balance for a system consisting of a thermal mass, C, and a thermal impedance of conductance, K (Weckmann, 1997). 25

2.6 Modified energy balance with heat of adsorption as the thermal energy source. 28

3.1 Microscope images of typical thermopile. 30

3.2 Diagram of assembled sensor (Guilbeau, 2008). 31

3.3 Diagram of testing system flow channel (Guilbeau, 2008). 31

3.4 Diagram of testing system flow apparatus (Guilbeau, 2008). 32

4.1 Response time test results. 34

4.2 Baseline testing for bare thermopile response to acetone. 35

4.3 Activated charcoal sensor response for repeatability testing. 36

4.4 Activated charcoal sensor response for linearity testing. 36

4.5 Activated charcoal sensor output versus time with repeating changes in acetone exposure levels. 37

4.6 Activated charcoal sensor output versus time with repeating changes in ethanol exposure levels. 38

4.7 Dow Corning High Vacuum Stopcock Grease sensor output with repeating changes in acetone exposure levels for repeatability testing. . 39

Figure Page
4.8 Dow Corning High Vacuum Stopcock Grease sensor output with repeating changes in acetone exposure levels. 40
4.9 Dow Corning High Vacuum Stopcock Grease sensor output with repeating changes in ethanol exposure levels. 41
4.10 Polydimethylsiloxane sensor output versus time with repeating changes in acetone exposure levels. 42
4.11 Polydimethylsiloxane sensor output versus time with repeating changes in ethanol exposure levels. 43
4.12 Polytetrafluoroethylene sensor output versus time with repeating changes in acetone exposure levels. 44
4.13 Polytetrafluoroethylene sensor output versus time with repeating changes in ethanol exposure levels. 45
5.1 Peak output data for acetone testing with each biorecognition material. 49
5.2 Peak output data for ethanol testing with each biorecognition material. 50

Nomenclature

A	Cross-sectional Area (m^2)
C	Heat capacity (J K^{-1})
C_p	Specific heat (J kg^{-1} K^{-1})
G	Gibbs Free Energy (kJ mol^{-1})
H	Enthalpy (kJ mol^{-1})
K	Thermal conductivity (W m^{-1} K^{-1})
k	Thermal conductance (W K^{-1})
k_a	Freundlich Adsorption Constant
L	Depth of the Absorber Layer (m)
m	Quantity of Adsorbent (g)
n	Number of Thermocouple Junction Pairs
n_a	Freundlich Adsorption Exponent
P	Pressure (kPa)
P_e	Radiative Energy (W), Heat Energy (W), Electrical Power (W)
P_0	Vapor Pressure above Adsorbate Layer
S	Entropy (kJ mol^{-1} K^{-1})
S_{AB}	Relative Seebeck Coefficient (V K^{-1})
t	Time (s)
T	Temperature (K)
x	Quantity of Adsorbate (mg)
V	Electrical potential (V)
V_{mono}	Volume of Monolayer Adsorbed Adsorbate (L)
V_{total}	Total Volume of Adsorbed Adsorbate (L)

Greek

μ	Micro
τ	Time constant (s)
θ	Number of Adsorption Sites

Chapter 1

INTRODUCTION

Exhaled human breath contains over 100 kinds of gases, of which many are used as biomarkers for monitoring physiological conditions (**?**). That is, the biomarkers can be analyzed to determine the presence or progression of several diseases. Whether the biomarkers are volatile organic compounds (VOC) produced by cellular processes or cancerous tumors, or rather inorganic compounds present as pollutants in the body, these chemical compounds provide insight into the physiological state of a subject. The motivation for the work described in this thesis is to contribute to the research conducted in breath analysis for acetone and ethanol detection. The present effort is aimed at exploiting adsorption thermodynamic principles for the development and characterization of thermoelectric-based breath analysis biosensors. The following section provides an introductory overview of this work.

Noninvasive Sensing

The movement towards noninvasive diagnostic sensing may have begun as early as the Renaissance, when DaVinci, Vesalius, and their contemporaries rejected the notion that dissection of the human body was inappropriate (Domach, 2004). Domach further states that from a technical standpoint, this paradigm shift was a significant step towards providing the basic information and framework with which to pose diagnostic questions and to interpret the results of tests. Centuries later, the desire to understand the mechanisms of physiological and pathophysiological conditions persists.

With significant advances in technologies, however, the ability to assess these conditions has grown exponentially, especially in the last fifty years. From

ultrasound and nuclear imaging to chemical and electrographic analysis, the medical diagnostic field continues to grow. Further, the demand for noninvasive medical devices, which do not require entering the body or puncturing the skin continues to develop as well.

There are two types of noninvasive devices to consider; therapeutic devices like those designed for cardiac defibrillation or radio therapy and diagnostic devices like those designed for electrocardiography or plethysmography. The benefits of noninvasive diagnostic testing, however, are touted to have the ability to revolutionize the medical device industry (Manohar, 2010). These benefits include improved quality of life for patients, reduced healthcare costs, and even earlier detection of diseases.

With these benefits in mind, the development of breath analysis techniques represents a distinct niche in the research and development of noninvasive medical devices. The International Association for Breath Research is at the forefront of the these effort, working in global collaboration with industry executives, entrepreneurs, investors, scientists and clinicians to promote advancement of the field. There is no doubt that scientific research from several disciplines has contributed to the development of novel methods for analyzing breath. Novel and original work has been generated nationally, from government agencies like the National Aeronautics and Space Administration and the Environmental Protection Agency to academic institutions like the University of California, Davis and the Cleveland Clinic. Since the start of the twenty-first century, these and other interested parties have collaborated at Meetings and Summits to discuss the trends, future directions, and technologies available for breath analysis.

Experimental Purpose

The focus of this work is directly related to breath analysis research for noninvasise diagnostic sensing. More specifically, the research objective was to determine the feasibility of an adsorption-based diagnostic biosensor for breath analysis. In particular, this work attempted to further the area of breath sensing, a noninvasive diagnostic sensing approach, by characterizing the performance of a thermoelectric gas sensor designed for acetone and ethanol detection.

Previous studies on thermoelectric gas sensors demonstrated the ability to detect chemical heats of reaction (Muehlbauer et al., 1989). Subsequent work in the area of thermoelectric gas sensing for breath sensing demonstrated the ability to detect chemical heats of reaction for acetone breath sensing applications (Guilbeau, 2008). In this research, the intention was to evaluate the heats of adsorption for acetone and ethanol sensing applications.

Review of Biosensor Device

Biosensors are often defined as devices that either use living organisms or biological molecules for detection. They are also defined as devices that detect information changes in biological systems. For the purposes of this work, the latter definition was most appropriate. Biosensors are also characterized by two components; a transduction component and a biorecognition component. The device evaluated in this research used a thermopile for thermoelectric transduction and one of four materials for biorecognition. These components are discussed in the ensuing sections.

Transduction via Thermoelectricity

The decision to use a thermoelectric transducer was based on an established history of using calorimetry for sensor design. In particular, thermopiles have been used to develop chemical biosensors. For instance, previous work with thermopiles has demonstrated that they can be used to detect the heat generated by enzymatic reactions (Muehlbauer et al., 1990a). In that case, thermopiles were used for glucose and urea testing. Alternatively, thermopiles have also been used in radiometry, the science of measuring thermal radiation. Thermal radiation, which is produced by accelerating charges and changes in electrical dipole moments of atoms and molecules in motion, has been characterized for understanding sun-earth energy exchanges (Weckmann, 1997).

An additional reason for choosing to use thin-film thermopiles was that they are highly sensitive to small changes in temperature and can respond with exceptionally small time constants. Thermopiles also generate their own electrical current, which make them inexpensive transduction elements. Past research attempts to improve sensor performance focused on increasing the temperature sensitivities and the signal-to-noise ratios by respectively implementing micromachine technology (Allison et al., 2003) and optimizing sensor placement and function (Towe and Guilbeau, 1996). Ultimately, developments in thermopile research to date confirm that this thermoelectric approach is certainly suitable for biosensor design.

Biorecognition via Heat of Adsorption

One mechanism for analyte device interaction has historically been adsorption. For instance, volatile organic compounds have been adsorbed for removal processing and detection testing. Adsorption describes the accumulation of a molecular

species or adsorbate at the surface of a liquid or solid phase in comparison to the bulk of the substrate. Adsorptive methods have been used in many applications. Activated charcoal has been used as a toxic gas remover in gas masks and silica gel has been used as a desiccator for chemical processes. Adsorption has also been used to perform heterogeneous catalysis. For this work, adsorption was used as an indicator for chemical detection.

It is believed that the thermodynamic properties for this process, in particular, the heats of adsorption, can be detected using various biorecognition materials. The choice of biorecognition material was based on the adsorption properties it exhibited. Acetone and ethanol have been characterized often for adsorption by activated charcoal. In fact, the deformation of activated carbon upon adsorption has been investigated since 1927 (Balzer et al., 2011). With such an extensive history of use, it was chosen as one of the biorecognition materials.

Polydimethylsiloxane (PDMS), a polymeric organosilicon or silicone, was also used. PDMS is often used as stopcock grease in wet chemistry laboratories and in soft lithography for microfluidics. In terms of chemical structure, PDMS in its semisolid form, a grease, and PDMS in its solid form, a cured elastomer, are known to have hydrophobic surfaces and are often used to provide barriers for aqueous solvents. While some mixtures of water and alcohol do not deform PDMS, most organic solvents do cause PDMS to deform. Because of its chemical properties, PDMS in both forms was chosen for two of the biorecognition materials.

Lastly, polytetrafluoroethylene (PTFE), a synthetic fluoropolymer of tetrafluoroethylene, was chosen. As a type of control material, it was believed that PTFE would have less interaction with the adsorbates than the other three materials. Though often used for lubricants as an ultra-high-molecular-weight, low friction polyethylene, PTFE's high corrosion resistance, biocompatibility, and hydropho-

bicity were the properties that made PTFE an attractive biorecognition material. Therefore, it too was chosen as a biorecognition material for testing. Combined with the transducer, each material was used to investigate heats of adsorption for acetone and ethanol.

Clinical Significance of Biosensor Device

The decision to test acetone and ethanol in the breath was based on the clinical significance of both analytes. While acetone is clinically relevant in the management of diabetes and obesity, ethanol is relevant to both medical testing and the legal implications of alcohol consumption. For instance, acetone is key marker for assessing the condition, diabetic ketoacidosis. Diabetic ketoacidosis occurs when acid levels in the blood rise due to the metabolism of fat-based ketone bodies over the metabolism of carbohydrates in insulin deficient individuals. While diabetic ketoacidosis can be lethal for diabetic patients, it is a physiologic condition that, under control, is highly sought after for managing obesity. In such instances, acetone in the blood or urine may be tested to asses a patient's level of ketone production. On the other hand, ethanol blood tests are regularly conducted to assess ethanol toxicity and alcohol related injuries. The prevalence and implications of each related issue make acetone and ethanol significant analytes for study.

As an example, the prevalence of diabetes in the United States is staggering with over 25% of United States residents aged 65 years and older diagnosed. Further, complications from diabetes can be life threatening. Diabetes has been found to be the leading cause of kidney failure, non-traumatic lower-limb amputation, and new cases of blindness among adults in the United States. It is a major cause of heart disease and stroke, as well as the seventh leading cause of death in the United States (CDC, 2011).

Additionally, in the United States, more than 33% of adults and more than

17% of children are considered obese (CDC, 2010). The growth in obesity from 1980 through 2008 for adults doubled and for children tripled. Moreover, these obesity rates were found to cross all groups in society – regardless of age, sex, race, ethnicity, socioeconomic status, education level, or geographic region. Ketogenic diets have been prescribed for managing obesity and even pediatric epilepsy. With these diets, ensuring that the ketosis condition caused by ketogenic lipolysis never becomes ketoacidosis is critical. Acetone, one of the three ketone bodies produced by the liver during the state of ketosis is therefore a useful biomarker.

With respect to alcohol and alcohol related injuries, a global issue was identified. In 2005, it was determined that alcohol causally related to more than sixty different medical conditions, in most but not all cases detrimentally (Room et al., 2005). In the clinical setting, ethanol testing was originally conducted using blood tests to determine intoxication levels. Analysis of breath for alcohol, however, has been practiced for the pre-clinical diagnosis of intoxication for more than seventy years (Dubowski, 1991).

Breath alcohol analysis has been detected via chemical oxidation and photometry, electrochemical oxidation via fuel cell technology, gas chromatography, infrared spectrophotometry, and even solid state semiconductor sensing. For the purposes of this work, ethanol was detected via thermoelectric principles. In particular, the thermoelectric sensor under investigation was constructed using a thermopile for transduction and four different materials for biorecognition in a simulated breath environment.

The clinically significant analytes, acetone and ethanol, were evaluated under dry air and humidified air conditions. The sensor response to acetone concentration was evaluated for repeatability and linearity, while the sensor response to ethanol presence was evaluated for repeatability. The different biorecognition materials were characterized based on their thermoelectric response to each ana-

lyte. Ultimately, a feasibility study on the thermoelectric biosensor was conducted to determine the likelihood of using adsorptive chemistry for analyte recognition.

Chapter 2

BACKGROUND and THEORY

The purpose of this section is to review background information on the proposed mechanism for heat generation in the sensor, adsorption. Additionally, a proposed model for the heat of adsorption is presented. Lastly, a review of methods for measuring heats of adsorption is discussed.

Adsorption Fundamentals

Adsorption is defined as a phenomenon of mass accumulation. A molecular species accumulates at the surface of liquid phase or solid phase, the substrate or adsorbent. The accumulated volume is small in comparison to the bulk of the substrate. This process occurs, because attractive intermolecular forces exist at the surface of the substrate. The unbalanced or residual forces attract the molecular species to the surface of the substrate. Adsorption is a surface phenomenon that is unlike absorption, in that the latter involves mass accumulation in the bulk medium.

Absorption, a bulk process, occurs when a molecular species is uniformly distributed within the bulk of the substrate. It is important to note that there exists another process that must be defined, sorption. Sorption is defined as a process in which both adsorption and absorption processes occur together.

Further, adsorption is characterized as a spontaneous process. Thus, a decrease in free energy, ΔG, occurs and ΔG for the system is a negative number. Further, the randomness of the system also decreases. Therefore, ΔS is also negative. With these thermodynamic parameters reviewed, it is possible to consider the enthalpy of the reaction.

Recalling basic thermodynamic principals whereby $\Delta G = \Delta H$ - $T\Delta S$, the

basic equation can be modified accordingly. $\Delta G = \Delta H + T\Delta S$ now allows for an assessment of enthalpy. For the equation to be true, ΔH must be negative as $-\Delta G - T\Delta S = \Delta H$, and the reaction must be considered exothermic.

Adsorption is indeed an exothermic process. The process of adsorbents adsorbing onto an adsorbate represents a host of changes in intermolecular and inter-atomic forces. Ultimately, the forces of attraction between the adsorbate and the adsorbent yield enough change in energy that the interaction produces a measurable heat of adsorption.

Types of Adsorption

There are two types of adsorption that exist. Chemical adsorption and physical adsorption are the two types of adsorption, and they differ by the forces of attraction that govern the interaction between the adsorbent and and adsorbate. For chemical adsorption, chemical bonds represent strong forces of attraction. On the other hand, physical adsorption can be defined by weaker forces like London forces or Van der Wall forces. Due to the different mechanisms involved in both types of adsorption, there are different corresponding heats of adsorption.

The heats of adsorption for chemical and physical adsorption are on the order of 200-400 kJ mol^{-1} and 20-40 kJ mol^{-1} respectively. Additionally, the effect of temperature on the both types of adsorption varies as well. For chemical adsorption, the relationship between extent of adsorption and temperature exhibits a parabolic behavior. Chemical adsorption increases with temperature and then decreases. Physical adsorption, instead, decreases exponentially with increasing temperature. These trends are demonstrated below in Figures 2.1 and 2.2. In both Figures, the extent of adsorption is defined by the term x/m, where x is the amount of adsorbate and m is the amount of adsorbent.

Independent of the different types of adsorption, there are four key fac-

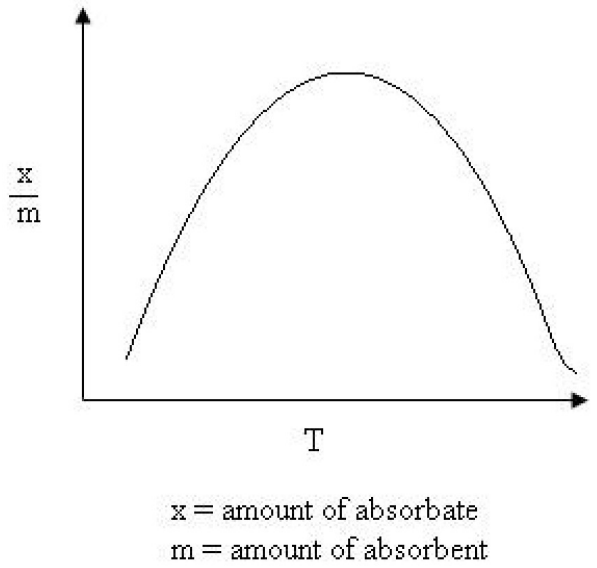

Figure 2.1: Relationship between chemical adsorption and temperature (Sharma and Singh, 2011).

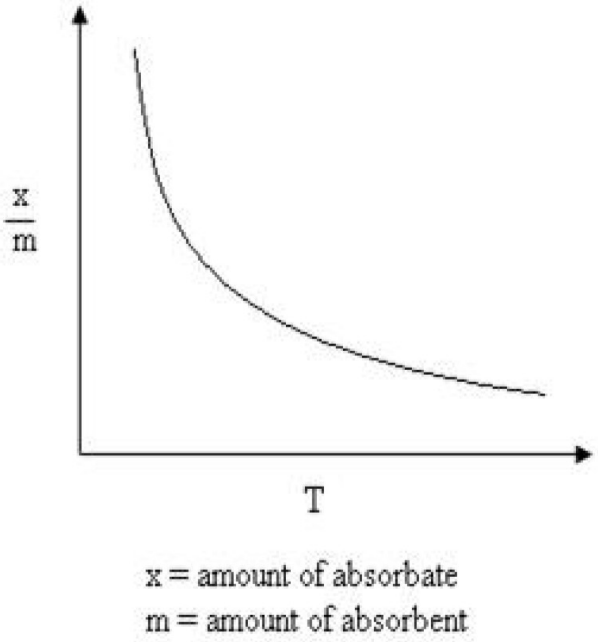

Figure 2.2: Relationship between physical adsorption and temperature (Sharma and Singh, 2011).

tors that impact adsorptive process. Temperature, pressure, surface area, and adsorptive properties of the adsorbent. For the purposes of this work, physical adsorption was assumed to be the governing interaction between the analytes, acetone and ethanol, and the biosensor. Under this assumption it was useful to investigate how adsorption is measured and experimentally characterized.

Theoretical Foundations for Describing Adsorption

Adsorption is often evaluated using adsorption isotherms. Isotherms are representations of equilibrium adsorptive processes that depict the amount of adsorbate on a surface versus the pressure of the system at constant temperature. Prominent examples of these isotherms include the Freundlich, the Langmuir and the Brunauer, Emmett and Teller (BET) isotherm theories. While each theory varies from the others, they are each based on equilibrium principles. It is useful to describe the adsorption process as a chemical reaction.

$$\text{Adsorbate} + \text{Adsorbate} \rightleftarrows \text{Adsorption Product}$$

From the reaction shown above, one can apply general chemistry principles for systems at equilibrium.

Le Châtelier's Principle for instance, states that a system will shift in such a manner so that it may relieve an applied stress. In this case, an increase in the pressure of a system tends to shift the equilibrium so that the number of moles of gas in a system decreases. In another example, increasing the temperature of an exothermic reaction will shift the reaction to the left while increasing the temperature of an endothermic reaction will shift the reaction to the right.

These basic principles can also be applied to adsorption. This is what Freundlich, Langmuir, Brunauer, Emmett and Teller (BET) attempted to do in their work. In 1909, Freundlich presented an empirical expression that represented

the isothermal variation of adsorption. In particular, the amount of adsorbate adsorbed by unit mass of adsorbent was evaluated by pressure. The resulting correlation was defined as the Freundlich adsorption isotherm model or equation.

$$\frac{x}{m} = k_a P^{\frac{1}{n_a}} \tag{2.1}$$

Here, x is still the mass of the gas adsorbed on mass, m, of the adsorbent at pressure P. Meanwhile, k_a and n_a are constants that are dependent on the adsorbate gas at particular temperature. The Freundlich adsorption isotherm model was able to correctly establish the characteristic relationship of adsorption with pressure in low pressure settings. Yet still, the Freundlich adsorption isotherm model was unable to predict the relationship of adsorption with pressure in higher pressure settings.

However, nearly one hundred years ago and almost ten years after Freundlich, Langmuir proposed an alternative adsorption isotherm model, that is today called the Langmuir adsorption isotherm model. The Langmuir adsorption isotherm model is based on alternative assumptions. One of these assumptions is that adsorption occurs such that only a single layer of adsorbate adsorbed on the adsorbent. Most significant, however, is the assumption that a dynamic equilibrium exists between adsorbed gaseous molecules and free gaseous molecules. To assess this concept, the following reaction equation is useful to consider.

$$A(g) + B(s) \rightleftarrows AB$$

In the reaction equation, $A(g)$ represents the free gaseous molecule, $B(s)$ represents the unoccupied solid surface of the adsorbent, and AB represents the adsorbed gaseous adsorbate molecule.

By developing the Langmuir Adsorption theory, Langmuir derived an equation that recognized a relationship between the number of active sites of the surface available and participating in the adsorption process adsorption at a given

pressure. With the introduction of two new variables, the Langmuir Adsorption equation, shown below in Equation 2.2, was able to better characterize the adsorption phenomenon.

$$\theta = \frac{KP}{1 + KP} \tag{2.2}$$

The new Langmuir variable, θ, represents the number of sites of the surface of the adsorbent that are covered by gaseous adsorbate molecules. Still, P continues to represent pressure, while K represents the equilibrium constant for the adsoprtion and desorption process that occurs between the adsorbate in the gas phase and the surface of the adsorbent.

Limitations of Langmuir adsorption isotherm equation arise, because it is known to only be valid at low pressures. Specifically when lower pressures are evaluated, KP is small enough that, the denominator value, $1 + KP$, can be considered simply, 1. With the denominator, ignored, the Langmuir adsorption isotherm model is reduced to a simpler equation.

$$\theta = KP \tag{2.3}$$

On the other hand, at high pressures, when the value of KP is significantly large, that numerator and the denominator are relatively equal in value. In this case, the Langmuir adsorption isotherm model is simplified once more.

$$\theta = \frac{KP}{KP} = 1 \tag{2.4}$$

Collectively, these equations are often represented in graphical representations, also called isotherms. A sample isotherm that can be explained using Langmuir adsorption isotherm theory is shown in Figure 2.3. This graph represents a monolayer adsorption where only a single layer of adsorbate forms on the adsorbent. The isotherm in Figure 2.3 could be an example of the adsorption of

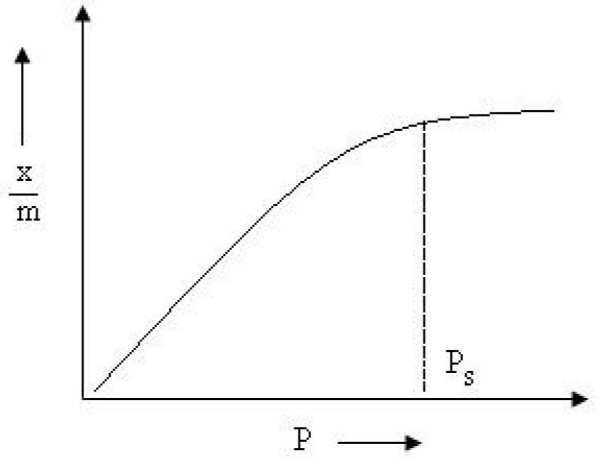

Figure 2.3: Sample isotherm generated from Langmuir theory (Sharma and Singh, 2011).

Nitrogen or Hydrogen gas on charcoal at temperatures near -180^{o}C (Sharma and Singh, 2011).

Alternatively, BET theory, created by Brunauer, Emmett and Teller sought to explain multilayer adsorption. The BET theory proposed that with multilayer adsorption, where more than one layer of adsorbate formed on the adsorbent, represented a more realistic characterization of the physical adsorption process. The difference in the theories is best evaluated at the limitation of the Langmuir adsorption isotherm model.

In particular, the Langmuir adsorption isotherm equation is valid at low pressures, when gaseous adsorbent molecules characteristically have high thermal energy and escape velocity. In this condition, fewer gaseous adsorbate molecules are available near the solid adsorbate surface. However, at high pressure and low temperature, the thermal energy of gaseous adsorbate molecules decreases with increasing number of gaseous adsorbate molecules available for interaction with the solid adsorbate surface. Under these condition, multilayer adsorption was proposed to occur and was characterized by the BET adsorption isotherm model

noted in Equation 2.5.

$$V_{total} = \frac{V_{mono} C \left(\frac{P}{P_0}\right)}{\left(1 - \frac{P}{P_0}\right)\left(1 + C\left(\frac{P}{P_0}\right) - \frac{P}{P_0}\right)} \tag{2.5}$$

In Equation 2.5, V_{total} represents the total volume of adsorbed material covering the surface of the adsorbent, while V_{mono} represents the total volume of adsorbed material forming a monolayer that covers the surface of the adsorbent. Additionally, the variable, C, represents the ratio of the equilibrium constant for a single molecule that is adsorbed on a vacant site of the solid adsorbent surface and the equilibrium constant for the saturated vapor liquid equilibrium.

$$C = \frac{K_1}{K_l} \tag{2.6}$$

In an alternative form, the BET equation, Equation 2.5, can be rearranged. This new arrangement is shown in Equation 2.7.

$$\frac{P}{V_{total}\left(P - P_0\right)} = \frac{1}{V_{mono} C} + \frac{c - 1}{V_{mono} C}\left(\frac{P}{P_0}\right) \tag{2.7}$$

The aforementioned BET adsorption isotherm equation can then used to create isotherms like the one defined by Langmuir adsorption isotherm model shown in Figure 2.3. For example, the isotherm shown in Figure 2.4, can be explained using BET adsorption isotherm theory which represents monolayer adsorption followed by multilayer adsorption. In this case, the sample graph might represent BET-characterized adsorption formed when Nitrogen gas is adsorbed at -195^{o}C on an Iron catalyst or silica gel (Sharma and Singh, 2011).

The information from isotherms like the ones just discussed are key to optimizing chemical engineering processes. For instance, in chemical batch adsorber processing, it is required that the adsorbent properties, isotherms, mass-transfer kinetics as well as fixed-bed dynamics be considered during the process and handling design. For the purposes of this work, these isotherms represent the bridge

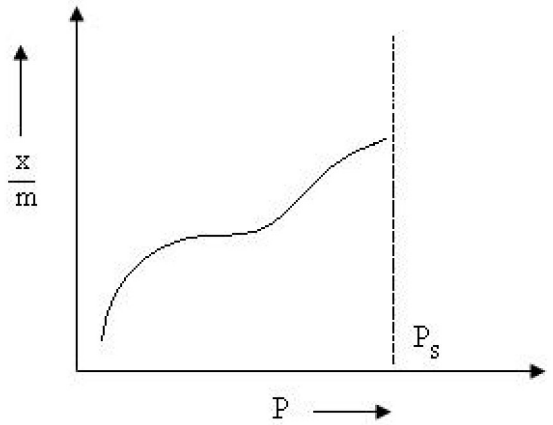

Figure 2.4: Sample isotherm generated from BET theory (Sharma and Singh, 2011).

toward defining the thermodynamics of adsorption. In particular, they are useful in determining isoteric heats of adsorption.

Thermodynamic Principles for Describing Adsorption

From a thermodynamic standpoint, the biosensor exploits the heat of adsorption of an analyte on a biorecognition material. For this reason, it was important to understand how the thermodynamic principles govern adsorption. In particular, the focus was on enthalpy and iosteric heat of adsorption.

It has been said that the Clausius-Clapeyron equation, is widely used to calculate the isoteric heat of adsoprtion (Pan et al., 1998). The Clausius-Clapeyron equation relates the adsorption heat effects to the temperature dependence of adsorption isotherms. To do so, there are two key assumptions made. The first assumption is that the bulk gas phase containing the gaseous adsorbate molecules is considered ideal. The second assumption is that the adsorbed phase volume is negligible by comparison.

While there are other methods for determining the isoteric heat of adsorption that consider other assumptions, a review of the theory described above is

presented (Pan et al., 1998). To begin, "the isoteric heat of adsorption q_{st} is defined as the differential change in energy δQ that occurs when an infinitesimal number of molecules δN are transferred at constant pressure, P, temperature T,and adsorbent surface area, A, from the bulk gas phase, G, to the adsorbed phase, a.

$$q_{st} = \left(\frac{\partial Q}{\partial N^a}\right)_{P,T,A} \tag{2.8}$$

A change in the integral heat of adsorption-dQ associated with an interfacial system is defined as

$$-\mathrm{d}q = T\mathrm{d}S \tag{2.9}$$

where the total entropy, S, is the sum of the entropies of the different phases

$$S = S^G + S^a + S^s \tag{2.10}$$

where S^G, S^a, and S^s are the entropies of the gas, adsorbed and solid phases, respectively. From a mass balance and assuming an inert adsorbent

$$\mathrm{d}N^G = -\mathrm{d}N^a \tag{2.11}$$

Based on equations 2.9 - 2.11, equation 2.8 is rewritten in the following form:

$$q_{st} = -T\left(\frac{\partial S}{\partial N^a}\right)_{P,T,A} = -T\left[\left(\frac{\partial S^G}{\partial N^G}\right)_{P,T} - \left(\frac{\partial S^a}{\partial N^a}\right)_{P,T,A}\right] \tag{2.12}$$

The total derivative of the chemical potential μ for the adsorbed phase is expressed as a function of P, T, and A:

$$d\mu^a = \left(\frac{\partial \mu^a}{\partial T}\right)_{P,A}\mathrm{d}T + \left(\frac{\partial \mu^a}{\partial P}\right)_{T,A}\mathrm{dP} + \left(\frac{\partial \mu^a}{\partial A}\right)_{P,T}\mathrm{dA} \tag{2.13}$$

From the Maxwell relations and noting that

$$\left(\frac{\partial \mu^a}{\partial T}\right)_{P,A} = -\left(\frac{\partial S^a}{\partial N^a}\right)_{P,T,A} \tag{2.14}$$

2.13 is rewritten as

$$\mathrm{d}\mu^a = -\left(\frac{\partial S^a}{\partial N^a}\right)_{P,T,A}\mathrm{d}T + V^a\mathrm{d}P + \left(\frac{\partial \mu^a}{\partial A}\right)_{P,T}\mathrm{d}A \tag{2.15}$$

where V^a is the adsorbed phase molar volume. For a bulk gas phase in equilibrium with the adsorbed phase

$$\mathrm{d}\mu^G = -\left(\frac{\partial S^G}{\partial N^G}\right)_{P,T} \mathrm{d}T + V^G \mathrm{d}P \tag{2.16}$$

where V^G is the gas phase molar volume. At a fixed adsorbed phase loading N^a and for a constant adsorbent surface area A, equating equations 2.15 and 2.16 leads to

$$\left(\frac{\mathrm{d}P}{\mathrm{d}T}\right)_{N,A} = \frac{\left(\partial S^G/\partial N^G\right) - \left(\partial S^a/\partial N^a\right)}{V^G - V^a} \tag{2.17}$$

Substituting equation 2.17 into equation 2.12 gives a general relation for q_{st} as

$$q_{st} = T\left(V^G - V^a\right)\left(\frac{\mathrm{d}P}{\mathrm{d}T}\right)_{N,A} \tag{2.18}$$

By neglecting the adsorbed phase molar volume and assuming an ideal gas for the bulk gas phase, equation 2.18 reduces to

$$q_{st} = RT^2\left(\frac{\mathrm{d}\left(\ln P\right)}{\mathrm{d}T}\right)_N \tag{2.19}$$

which is the familiar form of the Clausius-Clapeyron equation that is widely used in adsorption studies. When the isotherm is in the form $N = N(P,T)$, Equation 2.19 is changed to the following form by the chain rule of calculus:

$$q_{st} = -TV\left(\frac{\partial N}{\partial T}\right)_P \Big/ \left(\frac{\partial N}{\partial P}\right)_T \tag{2.20}$$

where $V = V^G - V^a$ and is calculated in different ways according to the different assumptions outlined" by the Pan method. (Pan et al., 1998).

Instead of evaluating the isoteric heat of adsorption, which is path dependent, it has been found advantageous to focus on enthalpy instead (Myers and Siperstein, 2001). Enthalpy, a state variable which is independent of path is also directly realated to the isoteric heat of adsorption for an ideal gas. With a perfect, ideal gas, the differential enthalpy of adsorption can be defined using Equation 2.19.

$$\Delta h = RT^2\left(\frac{\mathrm{d}\left(\ln P\right)}{\mathrm{d}T}\right)_N \tag{2.21}$$

Myers clarifies that the procedure used to produce Equation 2.19, where the isoteric heat of adsorption was obtained by differentiating a series of adsorption isotherms at constant loading N is still used today (Myers, 2002).

Myers also noted that whether the adsorption isotherm is determined experimentally or theoretically, thermodynamic properties can be calculated by numerical integration or differentiation and experimentally confirmed (Myers, 2004). As an example, differential also called molar enthalpy values for two multicomponent adsorption systems were compared to simulated values. These results showed that the simulated, modeled results correlated well with experimental values for the enthalpies (Myers and Siperstein, 2001).

Considering that the isoteric heat of adsorption, can be theoretically evaluated, it is worthwhile to consider how heats of adsorption can be experimentally measured. In the past, heats of absorption have been measured experimentally using calorimetry (Caspary et al., 1999). A similar approach was used to measure the heats of adsorption. In this case, the objective of the work was to consider a thermoelectric approach to measuring this heat of adsorption. In the ensuing section, a review of thermoelectric principles is provided with special attention given to thermopile devices.

Thermoelectric Phenomenon and the Thermopile

In the early 1980's, heats of adsoprtion were investigated using flow micro-calorimetry (Miwa et al., 1981). Additionally, heat generated by enzymatic reactions were determined using thermisters. By the 1990's, however, a new kind of calorimetric biosensor was reported that used thermopiles for measuring heats of reaction. (Bataillard et al., 1993; Guilbeau et al., 1987; Muehlbauer et al., 1990b). After twenty years, the thermopile approach is still a useful method for measuring thermodynamic properties, particularly enthalpies. The background and theory for

thermoelectric measurements using thermopiles is based on thermocouple technology. A review of this information is presented in the ensuing section.

Temperature measurement using thermocouple technology is based on the Seebeck effect. The amount of electrical potential produced can be interpolated as a measure of a temperature difference. This relationship is characterized by the electromotive force, emf, generated by an open circuit and a temperature difference between two junctions. The important factor in determining the activity of such a thermocouple is the choice of materials used for each thermoelement. For most applications, pairs of thermocouple elements that give a Seebeck voltage which varies with a high sensitivity to temperature are sought.

The transfer function for a thermocouple is determined by creating a calibration curve for the device. First the temperature at the reference junction is maintained at a fixed temperature. Meanwhile, the temperature at the other junction, the active junction, is varied. By plotting the sensor output with respect to known changes in temperature, the transfer function for the thermocouple is typically found to be linear while the slope of the transfer function represents the sensitivity of the device.

When considering the ideal thermocouple, that does not have problems with hysteresis, the slope of the calibration data can be evaluated to determine the Seebeck coefficient for the device. Since, the open-circuit voltage exhibits a linear relationship with the temperature difference between the junctions constructed by the two dissimilar metals, Metal A and Metal B, the Seebeck coefficient is essentially the slope. The typical equation for this relationship is shown in Equation 2.22 provided below (Weckmann, 1997).

$$\Delta V = S_{ab}(T)\Delta T \tag{2.22}$$

In this equation, S_{ab} is the relative Seebeck coefficient, expressed in V K^{-1}. The

Seebeck coefficient is dependent on the temperature difference as well as the electrical characteristics of the two dissimilar materials used. The sign of the Seebeck coefficient is determined based upon the sign of the voltage generated in relation to the temperature difference observed. The Weckmann approach uses absolute values to define the magnitude of the relative Seebeck coefficient. In this case, the magnitude of the relative Seebeck coefficient of a junction is calculated by taking the absolute value of the difference between Seebeck coefficients for each dissimilar metal. This concept is demonstrated in Equation 2.23 (Weckmann, 1997).

$$S_{ab} = |S_a - S_b| \tag{2.23}$$

One widely used application for thermoelectric devices is infrared detection. More specifically, multiple thermocouples in series, often coupled with a black-body radiation absorber, can be used to detect incident radiation. This is possible, because the voltage produced by the collective junctions represents the temperature difference that exists between the each paired junction. Sample paired junctions are shown in Figure 3.1, where each paired junction can be considered an individual thermocouple that can be used as a detector of incident radiation. For such a device, the open-circuit emf produced by a single junction pair is rather small relative to the total output for the device. Where the output for a single junction is on the order of a tenth of a microvolt per temperature difference in degree Celsius, the output for the entire device is proportional to the number of junctions in series (Weckmann, 1997). Thus, the output voltage of the entire device can be increased by increasing the number of junction pairs connected in series. More specifically, the sensitivity for the entire device is then increased by n when n thermocouple junction pairs are placed in series. This concept is represented in Equation 2.24.

$$\Delta V = nS_{ab}(T)\Delta T \tag{2.24}$$

The device just described is called a thermopile. A typical thermopile is shown in Figure 3.1. The Figure demonstrates that there are two dissimilar metals that form the active junctions, represented as C, and the reference junctions, represented as D. The Figure also demonstrates that the legs and junctions of the thermopile are connected as a series of thermocouples of alternating materials. They are the active junctions that are exposed to a heat source and produce a thermal equilibrium with the surroundings environment that is exposed to the reference junctions. Together, the observed temperature difference produces an emf at the leads, represented as A. Thermopiles have been evaluated for many applications. One important parameter that is often considered is thermopile sensitivity.

In particular, the sensitivity for thermopiles has been widely investigated and is dependent of the application of the thermopile. For a generic calorimeter, it has been recorded that a bulk micromachined silicon thermopile could achieve sensitivities as high as 500 mV $^{o}\mathrm{C}^{-1}$ (Allison et al., 2003) if 1000 junctions were used. The simplicity of design makes thermopile technology attractive for many applications. Provided in Table 2.1 is a summary of just a sample of applications and sensitivities documented in literature.

This work sought to use thermopiles to measure heats of adsorption. It is believed that theoretical characterizations for both the thermopile device and assembled sensor would correlate well with experimental data. The ensuring section provides an overview of the theoretical model used to describe the thermopile and the biosensor designed for acetone and ethanol detection.

Theoretical Model for Biosensor Device

To define a model for the biosensor device it was useful to consider the two-component system of the biosensor. First, the transduction component was con-

Application	Sensitivity	Source
Automotive Sensor	80 V W^{-1}	(Graf et al., 2007)
Generic Calorimetry	45 mV $^oC^{-1}$	(Allison et al., 2003)
Enzymatic Biochemical Sensor	5 mV $^oC^{-1}$	(Towe and Guilbeau, 1996)
	2 mV K^{-1}	(Xie et al., 1994)
Mast Cell Activation Sensosr	7 μW 10^6 cells	(Pizziconi and Page, 1997)
High Laser Power Measurement	2.8 mv W^{-1}	(Charles et al., 1988)
Thermal Radiation Detector	0.0543 mV $W^{-1}m^{-2}$	(Weckmann, 1997)
	6 V W^{-1}	(Herwaarden and Sarro, 1986)
	12.45 V W^{-1}	(Xue et al., 2010)
VOC Sorption Detection	nV ppm^{-1}	(Lerchner et al., 2000)

Table 2.1: Summary of thermoelectric applications using thermopiles.

sidered. Second, the biorecognition component was considered. Lastly, the two components were combined.

As a first step, the thermoelecric device was modeled as if it were an infrared detector. This approach was chosen, because it best represented the characterization approach used to investigate the response time of the thermopile.

To begin, the assumptions used in the Weckmann method were followed for this work. First, the thermopile, with its multiple junctions was considered as single one-junction thermopile. Second, the heat exchange generated by the incident radiant energy was defined as the heat input at T. Further, the heat exchange at the reference junction was represented the external environment, T_a. Here, the heat loss through conduction to the insulator and through radiation to the surrounding environment was considered negligible. Lastly, it was assumed that the initial temperature of the absorbing layer of the thermopile was the ambient temperature, the heat loss through radiation here was assumed to be

negligible, and the rate of absorption was assumed to be constant. Figure 2.5 shows the energy balance for this system. Identical to the Weckmann method,

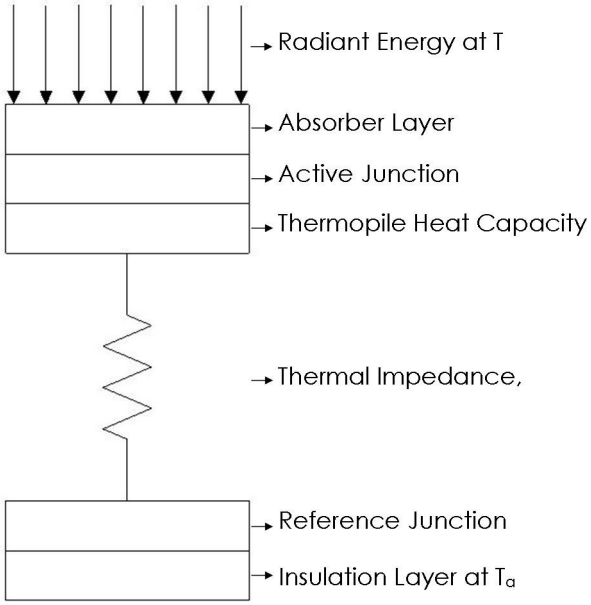

Figure 2.5: Energy balance for a system consisting of a thermal mass, C, and a thermal impedance of conductance, K (Weckmann, 1997).

the system described above lead to the energy balance presented below in the following equations. The first equation, Equation 2.25 defines the energy balance.

$$C\frac{d\Delta T}{dt} + K\Delta T = P_e \tag{2.25}$$

In Equation 2.25, P_e represents the incident radiant energy that contacts the absorber layer. Incident radiant energy is defined as power expressed in W. The thermal conductance of the absorber layer is defined then by K expressed in W K^{-1} between the thermopile and the heat source. Additionally, the heat capacity of the thermopile, C expressed in J K^{-1}, represents the thermal properties of the thermopile metals. The heat capacity of the thermopile is further characterized in Equation 2.26.

$$C = mC_p \tag{2.26}$$

Equation 2.26, demonstrates the basic relationship between the mass of the thermoelements, m expressed in kg, and their specific heat capacity, C_p expressed in J kg^{-1} K^{-1}. The thermal conductance of the absorber layer, K, which absorbs the incident radiant energy is also defined.

$$K = k\frac{A}{L} \tag{2.27}$$

In Equation 2.27, k is the conductivity of the of the absorber layer expressed in W m^{-1} K^{-1}, L is the depth of the absorber layer expressed in m, and A is the cross-sectional area of the absorber layer exposed to the radiant incident energy. The cross-sectional area is expressed in m^2.

By assuming that the rate of absorption was constant, the Weckmann method provided the solution to Equation 2.25. As such, Equation 2.25 could be written as it is shown below.

$$\Delta T = \frac{P_e}{K}\left(1 - e^{-\frac{K}{C}t}\right) \tag{2.28}$$

Here it is shown that an thermoelectric, thermopile-based radiation detector would have first-order system behavior and a time constant defined by τ.

$$\tau = \frac{C}{K} \tag{2.29}$$

By combining the results from Equations 2.24, 2.28, and 2.29, the relationship for the system can be written as it is below.

$$V = nS_{ab}\Delta T = nS_{ab}\frac{P_e}{K}\left(1 - e^{-\frac{t}{\tau}}\right) \tag{2.30}$$

Ultimately, the Weckmann method produces a means to theoretically assess the thermopile output for the device. In particular, the output voltage of is determined as before by multiplying the temperature differential across the reference and active junctions by the Seebeck coefficient, and the total number of junctions in the thermopile.

One of the characteristic parameters of the device is its sensitivity. The sensitivity for the thermopile can be theoretically defined by manipulating Equation 2.30.

$$\text{Sensitivity}=\frac{V}{P_e} = \frac{nS}{K}\left(1 - e^{-\frac{t}{\tau}}\right) \tag{2.31}$$

The sensitivity of the thermopile is essentially just the output voltage for the device divided by the power of the incident radiant energy. The sensitivity here is expressed in V (W m^{-2})$^{-1}$.

Another key parameter for the thermopile is the time constant of the thermopile. In most applications, it is advantageous to minimize the time response. One method to achieve this, is shown by inspection that thermal conductance of the system should be maximized while the heat capacitance of the thermopile should be minimized. On the other hand, maximum sensitivity can be achieved by maximizing the number of junctions in the thermopile, choosing dissimilar metals with large Seebeck coefficients, and alternatively minimizing the thermal conductance of the system.

Given the conflicting relationship with the thermal conductance, the Weckmann method suggests that the thermal conductance for the thermopile system must be optimized in order to achieve both maximum sensitivity and response time. For the purposes of this work, the Kapton layer, represented as B in Figure 3.1, is the absorber layer which is critical for determining device performance.

Physical adsorption was not modeled extensively. However, a cursory examination was attempted. In particular, the mass balance – energy balance for the system was simplified under basic assumptions. The first assumption was that the analyte was present in an ideal gas as a single-component. The second assumption was that the adsorbent was covered fully by only a single layer or monolayer of adsorbate. Further, the adsorption capacity of the adsorbent ex-

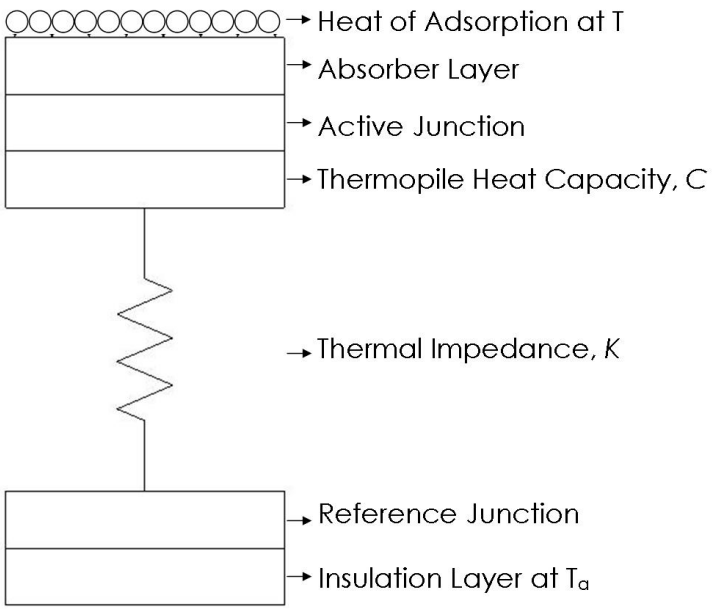

Figure 2.6: Modified energy balance with heat of adsorption as the thermal energy source.

hibited a linear relationship with the concentration of the adsorbate in the gas phase. The cursory model for this system is presented in Figure 2.6. With these assumptions identified, the isoteric heat of adsorption in the form of differentiated or molar enthalpy, would reach a maximum value once the adsorbate covered the the surface of the adsorbent. To model the proposed heat of adsorption, the absorber layer of the standard thermopile sensor was replaced by the biorecognition layer that generated heat.

Chapter 3

EXPERIMENTAL METHODS

The purpose of this section is to provide an overview of the experimental methods used for this work. A detailed review of the the device fabrication process is included. Additionally, the testing apparatus is also reviewed.

Thermopile and Biosensor Fabrication

The thermopiles were made using thin film deposition by thermal evaporation in a high vacuum bell jar system located in Arizona State University's LeRoy Eyring Center for Solid State Science. Bismuth and antimony were deposited on Dupont Kapton PV9100 series polyimide film. Bismuth and antimony shot from Sigma Aldrich underwent similar processes. In both cases, the metal was slowly heated under vacuum. The vapors then rose within the bell jar to condense on the Kapton film. The bismuth and antibody runs were conducted in three steps.

During the preliminary deposition of bismuth, one of two different metal shadow masks was used. Both masks were designed to create the patterns needed to fabricate each structure of the thermopiles. The masks were produced by Towne Technologies, Inc. of Somerville, New Jersey. A second metal shadow mask was used for the second bismuth run and the final antimony run. The alignment of the second masks to the previously deposited film was conducted visually under a backlight.

Once the runs were completed, the Kapton film was cut into individual thermopiles, analyzed by microscopy for defects and then assembled into sensor devices. The first step in the assembly process required that the thermopiles' electrical pads be fitted with adhesive-coated 3M 1181 copper foil tape. The electrical connections between the copper tape and thermopile pads were made

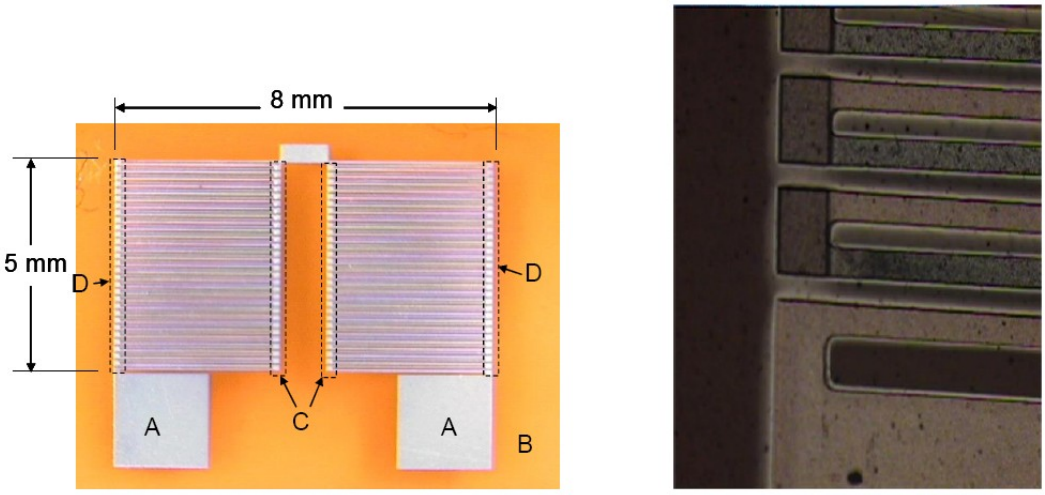

Figure 3.1: Microscope images of typical thermopile.

with GC Electronics Silver Print II, an electrically conductive silver paint.

The backsides of the thermopiles were modified to isolate the reference junctions. The reference junctions were protected by 3M 810 Scotch Magic Tape, while the backsides of the active junctions remained exposed. The thermopile devices were then trimmed and attached to their supporting substrates.

The supporting substrates were styrofoam-based, thermally insulated polyvinylchloride rings. The rings not only thermally isolated the frontside of the thermopiles, but also protected the thermopiles from mechanical damage. Finally, the active junctions were coated with a biorecognition material. The assembled sensors, demonstrated in Figure 3.2 were then ready for testing and placed in the flow channel shown in Figure 3.3. While there were many devices fabricated, the experiments presented in this thesis were conducted using one of two devices.

Biosensor Testing

The assembled sensor was first electrically connected to the testing system by using alligator clips that were attached to the positive and negative copper tape of the assembled device. Once electrically connected to the testing system, the

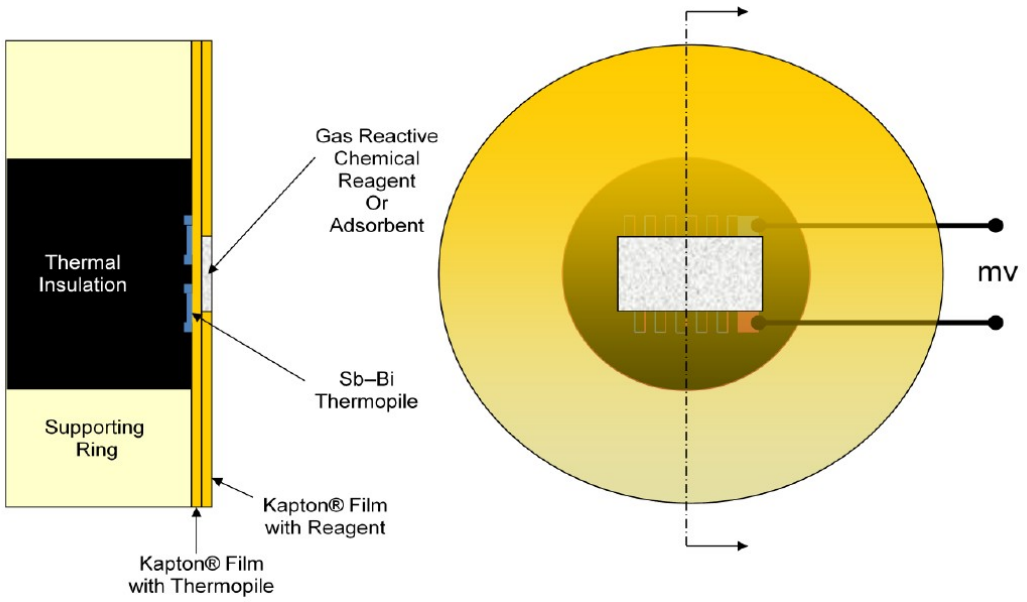

Figure 3.2: Diagram of assembled sensor (Guilbeau, 2008).

device was carefully placed in a flow channel like the one drawn in Figure 3.3. The flow channel was a key component of the testing system shown in Figure 3.4.

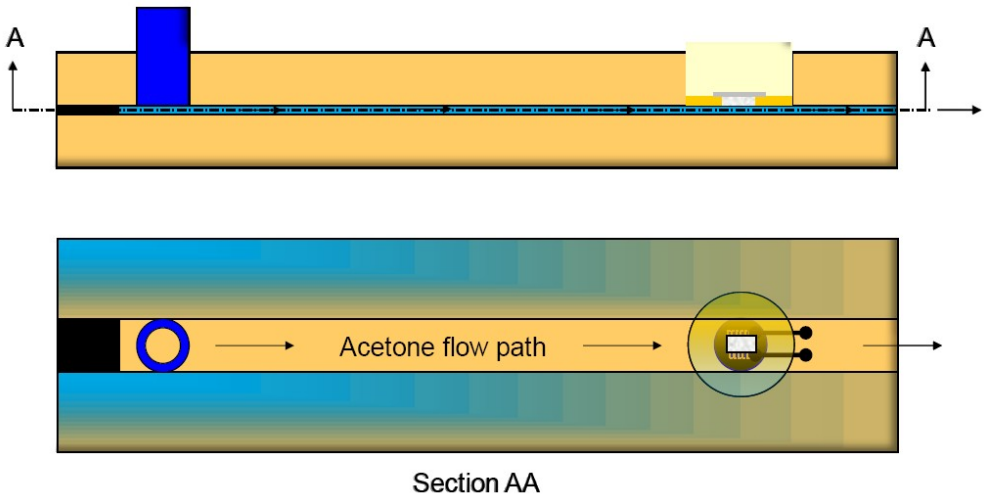

Figure 3.3: Diagram of testing system flow channel (Guilbeau, 2008).

The testing system consisted of a compressed air supply, two mass flow regulators, a humidifier, an analyte delivery station, a mixing chamber, a flow channel, and a null voltmeter. The compressed air was divided into two streams.

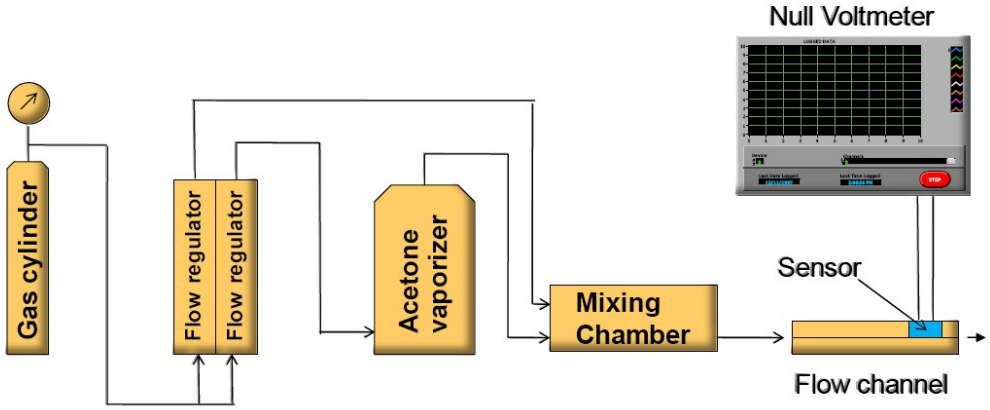

Figure 3.4: Diagram of testing system flow apparatus (Guilbeau, 2008).

One stream was sent through one of the mass flow regulators and on to the Bird Humidifier Controller that regulated both temperature and humidity. The second stream was sent through the other mass flow regulator and onto the analyte delivery station.

For acetone testing, the analyte delivery station was a Dräger Vapor 19.1 anesthetic agent delivery device that was modified for acetone vaporization. For ethanol testing, a conical flask, two-holed rubber stopper, and a glass dispersion tube were used to create an ethanol vaporization apparatus. The ethanol vaporization apparatus, unlike the acetone vaporization apparatus, did not allow for fine control of the analyte concentration in the airflow.

Irrespective of the analyte, the gas from the analyte delivery station was sent to a mixing chamber. From there, the gas flow from both mass flow regulators was mixed and sent on to the flow channel. In all experiments, the temperature was set to 25^{o}C.

Data Anlaysis

The objective of this research was to characterize the performance of a thermoelectric gas sensor designed for ethanol and acetone detection. This sensor was

evaluated by plotting real-time biosensor response during each experiment. The peak output data was used characterize the device repeatability and linearity. Additionally, the peak output data was used to compare biosensor response with varying biorecognition materials.

Chapter 4

RESULTS

This chapter is organized into three parts. The first part reviews the experimental results used to characterize the thermopile. The second part presents the experimental results for several biorecognition materials. Finally, in the third part, a review of theoretical results is discussed.

Transducer and Sensor Characterization

Device response to infrared incident light was evaluated to determine the response time of the device. The results are shown in Figure 4.1. The IR source used in this experiment was a standard Class IIIa office laser pointer with a 630-680 nm laser diode and a maximum power output rating at less than 5 mW.

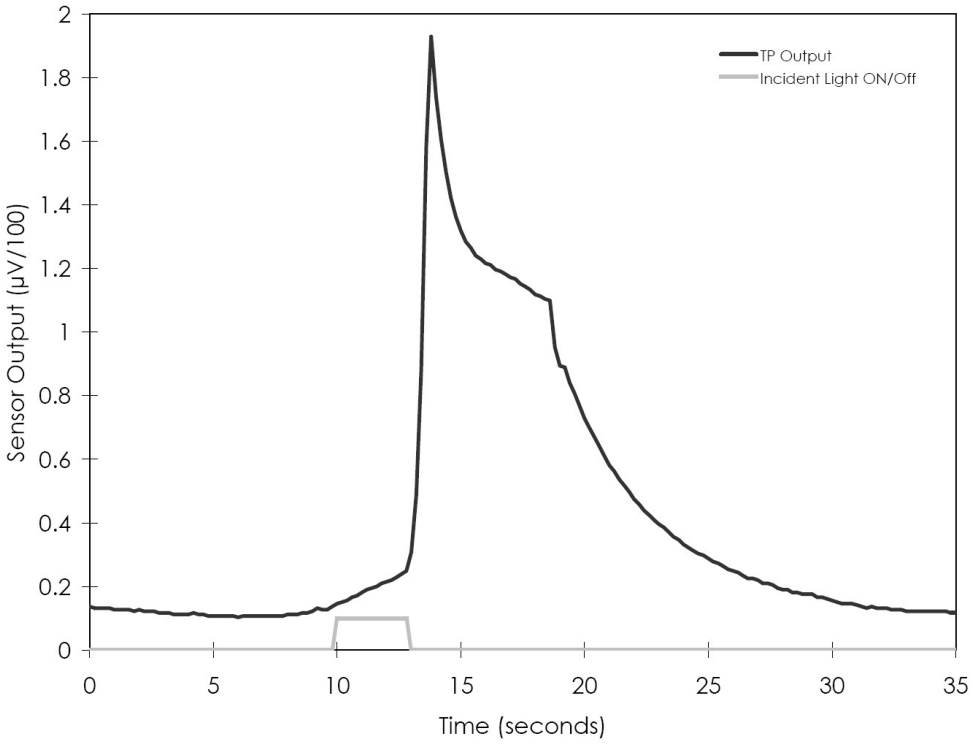

Figure 4.1: Response time test results.

A five minute baseline experiment was also run. This experiment was conducted to determine a baseline response to acetone. At 75 seconds, the sensor was exposed to a 7% acetone flow. The flow was returned to 0% acetone at 200 seconds. The results from this testing are presented in Figure 4.2

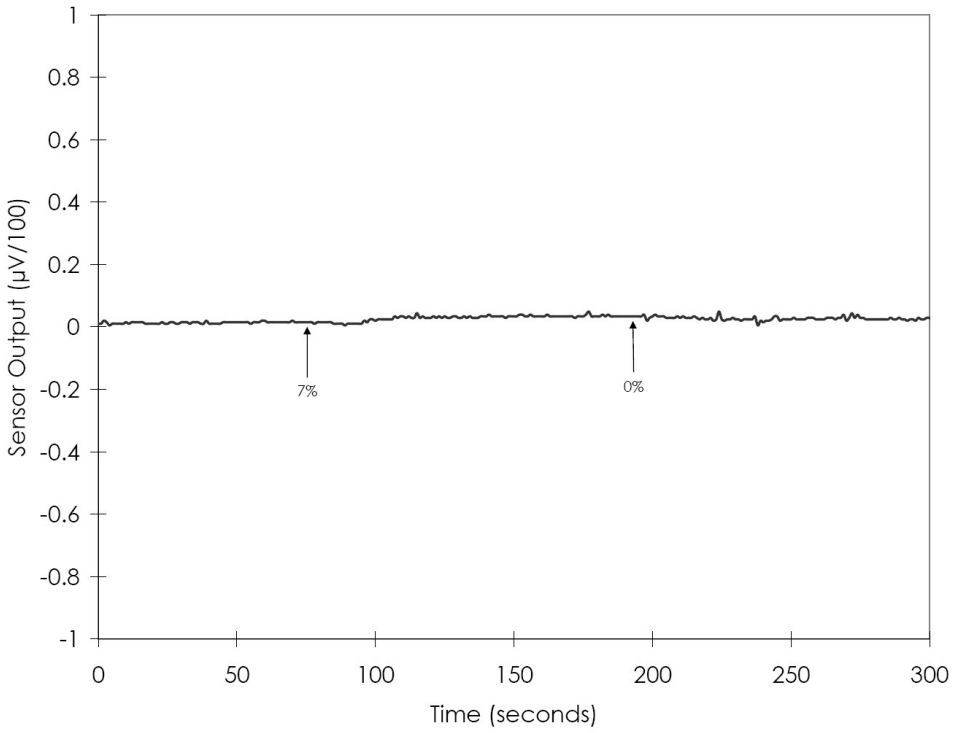

Figure 4.2: Baseline testing for bare thermopile response to acetone.

In addition to response time, and baseline testing, the assembled sensor was evaluated for repeatability. Using the most common adsorbent, activated charcoal, the sensor was evaluated in acetone at varying levels. The results from this study are presented in Figure 4.3. This data was also used to evaluate linearity. The results from this work are presented in Figure 4.4.

Biorecognition Material Evaluation

This testing was conducted in order to evaluate the biorecognition material response to varying concentrations of acetone and ethanol in both dry air and

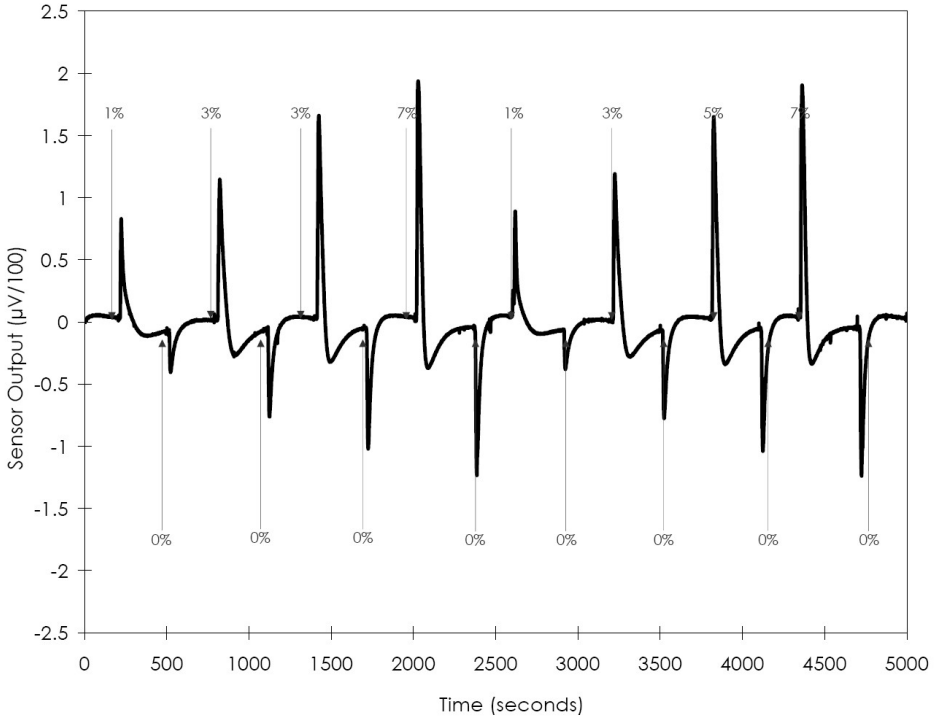

Figure 4.3: Activated charcoal sensor response for repeatability testing.

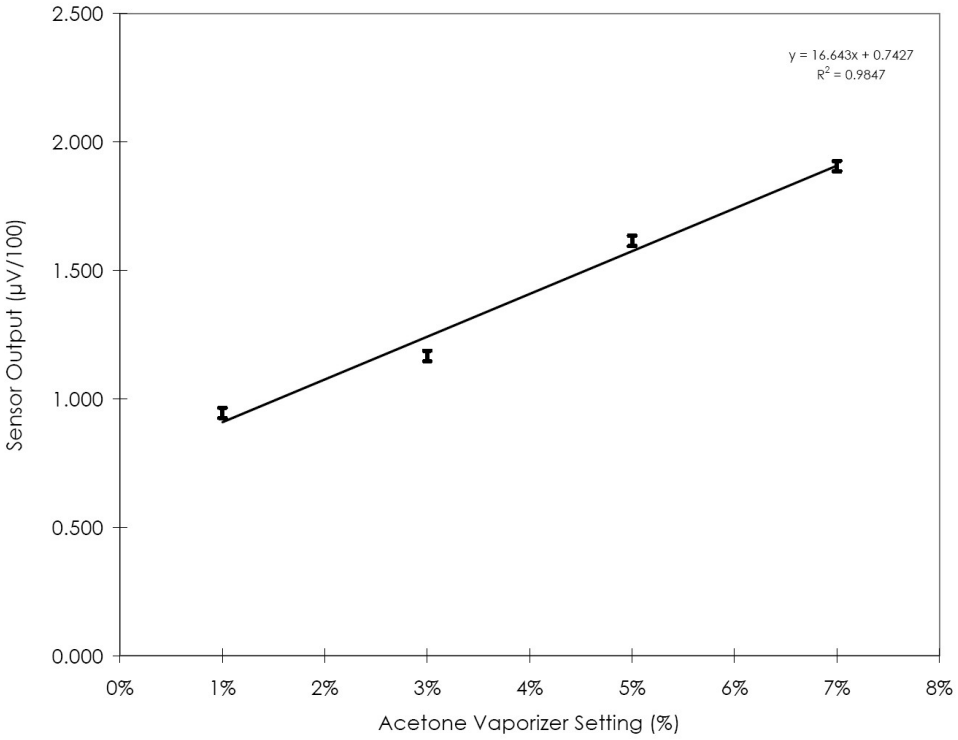

Figure 4.4: Activated charcoal sensor response for linearity testing.

humidified air. This section includes experimental results for four biorecognition materials: Activated Charcoal (AC), Semi-solid Polydimethylsiloxane in the form of Stopcock Grease (SCG), Solid Polydimethylsiloxane in the form of a cured elastomer (PDMS), and Semi-solid Polytetrafluoroethylene in the form of Krytox grease (PTFE).

Performance with Activated Charcoal

Each experiment was conducted in two parts. The first part was conducted in a non-humidified environment. The second part was conducted in humidified air. The biorecognition material was activated charcoal. For the acetone testing, Figure 4.5 presents the experimental data. The acetone concentration were varied amongst three values and data was collected twice before changing the ambient environment from dry to humidified.

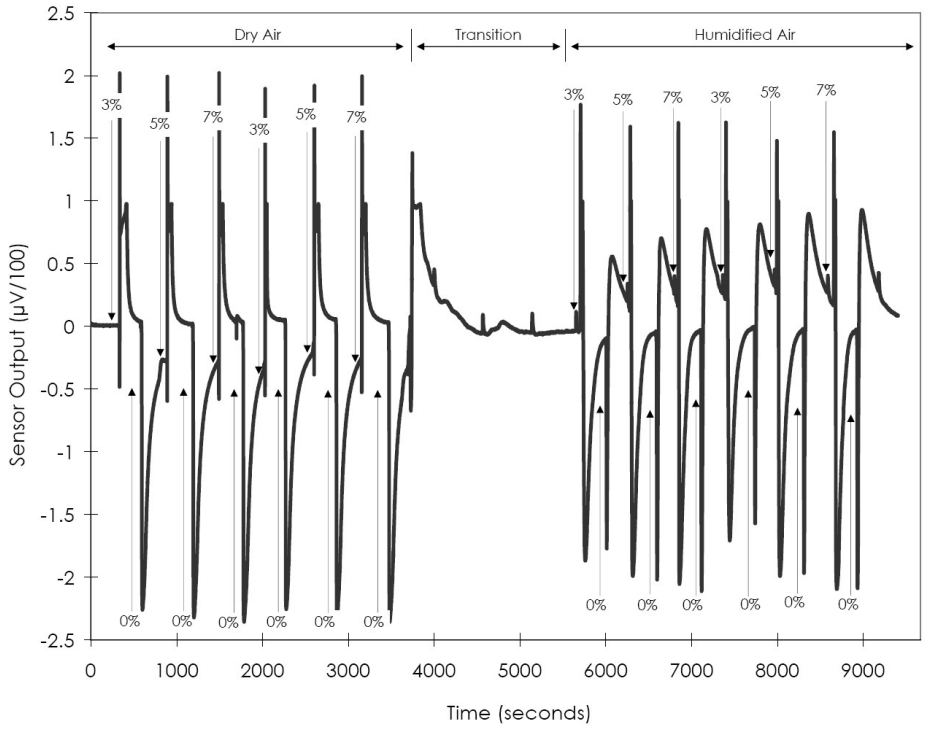

Figure 4.5: Activated charcoal sensor output versus time with repeating changes in acetone exposure levels.

As with the acetone testing, the ethanol testing was also conducted in two parts. The first part was again conducted in a non-humidified environment, while the second part was conducted in humidified air. The biorecognition material was still activated charcoal. For the ethanol testing, Figure 4.13 presents the experimental data. The ethanol was either present in the stream or completely absent. The data was collected three times before changing the ambient environment from dry to humidified

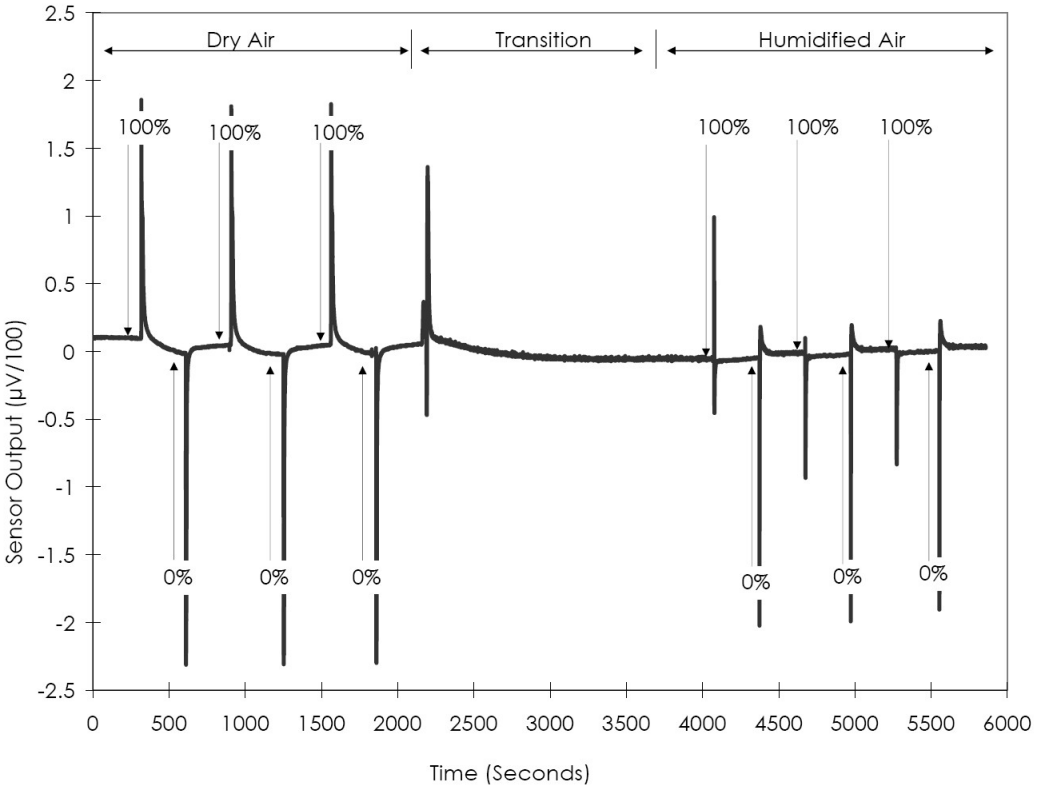

Figure 4.6: Activated charcoal sensor output versus time with repeating changes in ethanol exposure levels.

Performance with Semi-solid Polydimethylsiloxane

A repeatability study using stopcock grease (SCG) was also conducted. In a dry-air environment, acetone levels were varied to four settings. These settings were

sampled twice during the entire run. The results from these tests are shown in Figure 4.7.

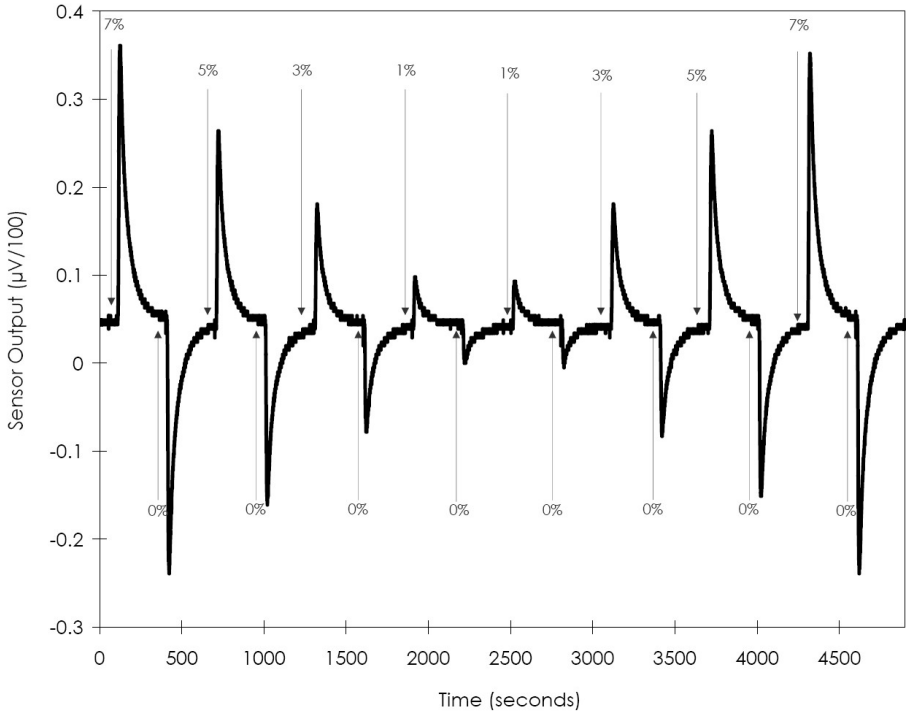

Figure 4.7: Dow Corning High Vacuum Stopcock Grease sensor output with repeating changes in acetone exposure levels for repeatability testing.

Once more, each of the remaining experiments were conducted in two parts. The first part was conducted in a non-humidified environment. The second part was conducted in humidified air. The biorecognition material was Dow Corning High Vacuum Stopcock Grease. For the acetone testing, Figure 4.7 presents the experimental data. The acetone concentrations were varied amongst three values and data was collected twice before changing the ambient environment from dry to humidified. In each experiment, only one biorecognition material, Dow Corning Stopcock Grease, was used.

As with the acetone testing, the ethanol testing was also conducted in two parts. The first part was again conducted in a non-humidified environment.

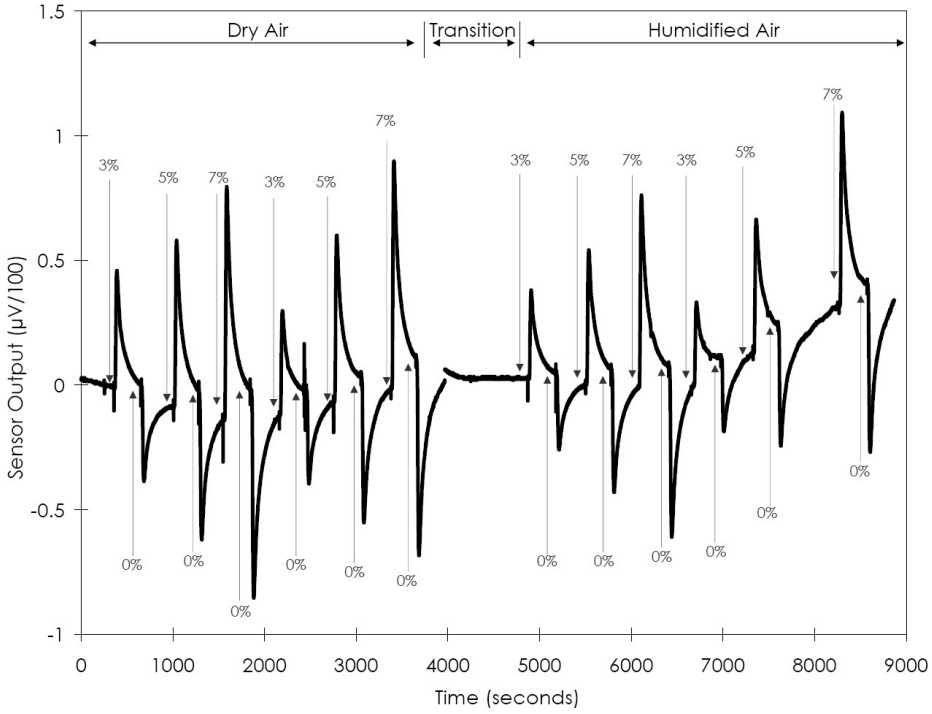

Figure 4.8: Dow Corning High Vacuum Stopcock Grease sensor output with repeating changes in acetone exposure levels.

The second part was conducted in humidified air. The biorecognition material remained Dow Corning High Vacuum Stopcock Grease. For the ethanol testing, Figure 4.9 presents the experimental data. The ethanol was either present in the stream or completely absent. The data was collected three times before changing the ambient environment from dry to humidified air.

Performance with Solid Polydimethylsiloxane

The PDMS testing followed the previous testing regime as well. Again, each of the experiment was conducted in two parts. The first part was conducted in a non-humidified environment. The second part was conducted in humidified air. The biorecognition material was solid polydimethylsiloxane that had been cured. For the acetone testing, Figure 4.10 presents the experimental data. The acetone concentrations were varied amongst three values and data was collected

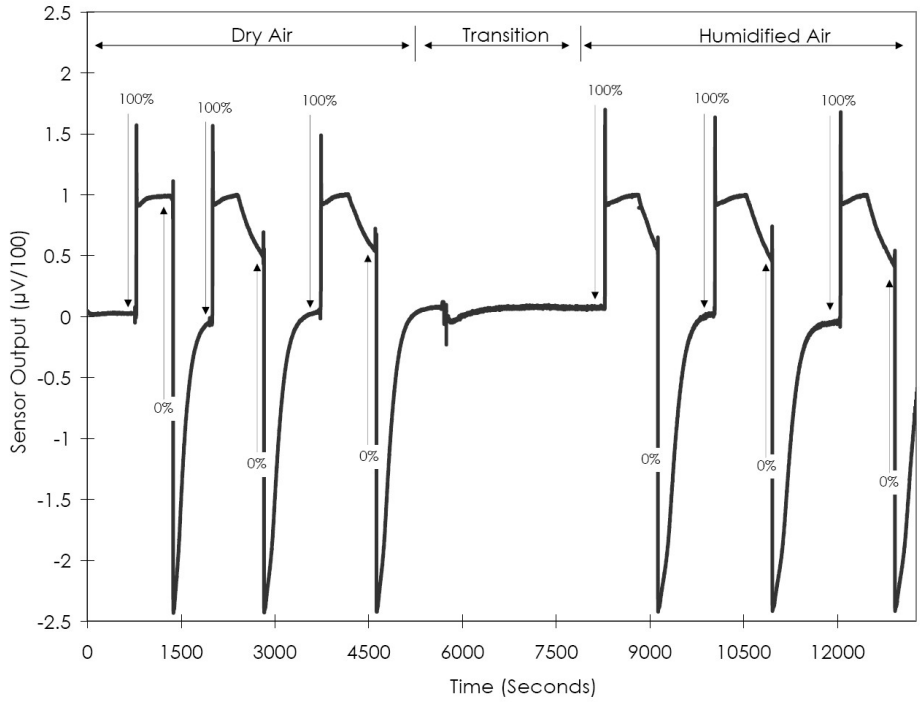

Figure 4.9: Dow Corning High Vacuum Stopcock Grease sensor output with repeating changes in ethanol exposure levels.

twice before changing the ambient environment from dry to humidified. In each experiment, only one biorecognition material, polydimethylsiloxane, was used.

As with the acetone testing, the ethanol testing was also conducted in two parts. The first part was again conducted in a non-humidified environment. The second part was conducted in humidified air. The biorecognition material was polydimethylsiloxane. For the ethanol testing, Figure 4.11 presents the experimental data. The ethanol was either present in the stream or completely absent. The data was collected three times before changing the ambient environment from dry to humidified air.

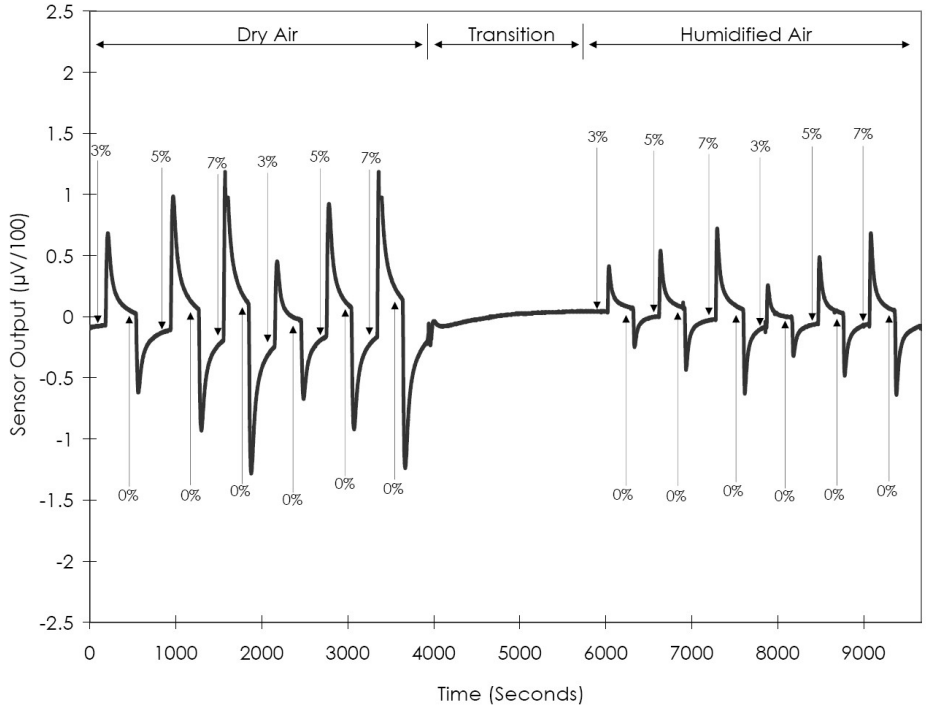

Figure 4.10: Polydimethylsiloxane sensor output versus time with repeating changes in acetone exposure levels.

Perfomance with Semi-solid Polytetrafluoroethylene

The polytetrafluoroethylene testing followed the previous testing regime as well. Again, each of the experiments were conducted in two parts. The first part was conducted in a non-humidified environment. The second part was conducted in humidified air. The biorecognition material was polytetrafluoroethylene. For the acetone testing, Figure 4.12 presents the experimental data. The acetone concentrations were varied amongst three values and data was collected twice before changing the ambient environment from dry to humidified. In each experiment, only one biorecognition material, polytetrafluoroethylene, was used.

As with the acetone testing, the ethanol testing was also conducted in two parts. The first part was again conducted in a non-humidified environment. The

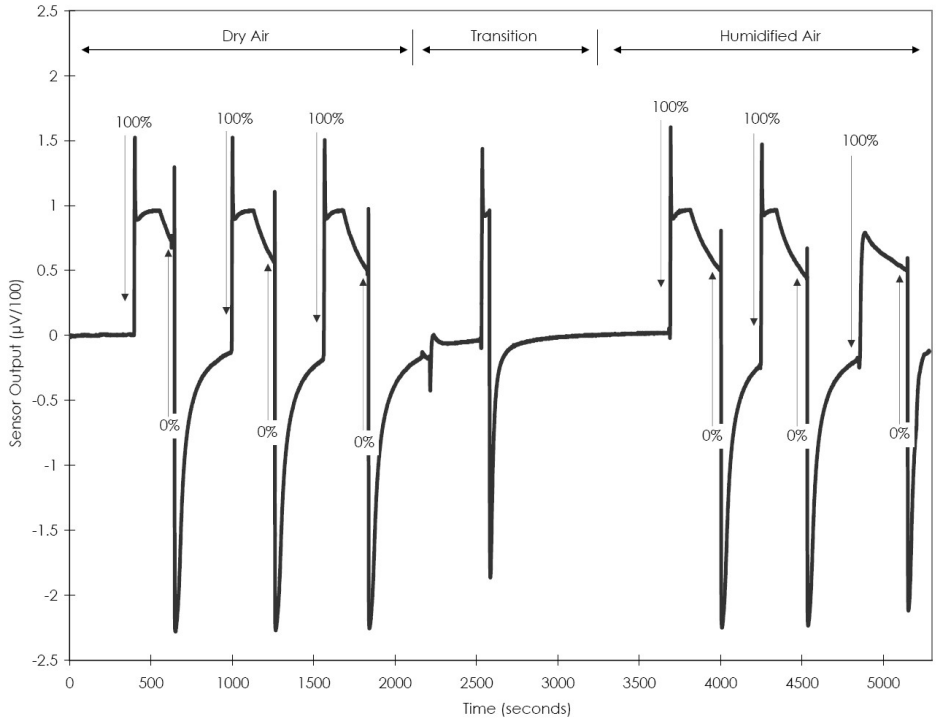

Figure 4.11: Polydimethylsiloxane sensor output versus time with repeating changes in ethanol exposure levels.

second part was conducted in humidified air. The biorecognition material was polytetrafluoroethylene. For the ethanol testing, Figure **??** presents the experimental data. The ethanol was either present in the stream or completely absent. The data was collected three times before changing the ambient environment from dry to humidified air.

Theoretical Model Validation

For the thermoelectric infrared sensor, the energy balance described in Figure 2.5 was evaluated. The sensitivity was found to be 7.2 μV m^{o}C^{-1}. The sample calculations for this work are provided in the Appendix. For the thermoelectric heat of adsorption sensor, the proposed energy balance was not experimentally validated. A discussion of this work is provided in the Discussion Section.

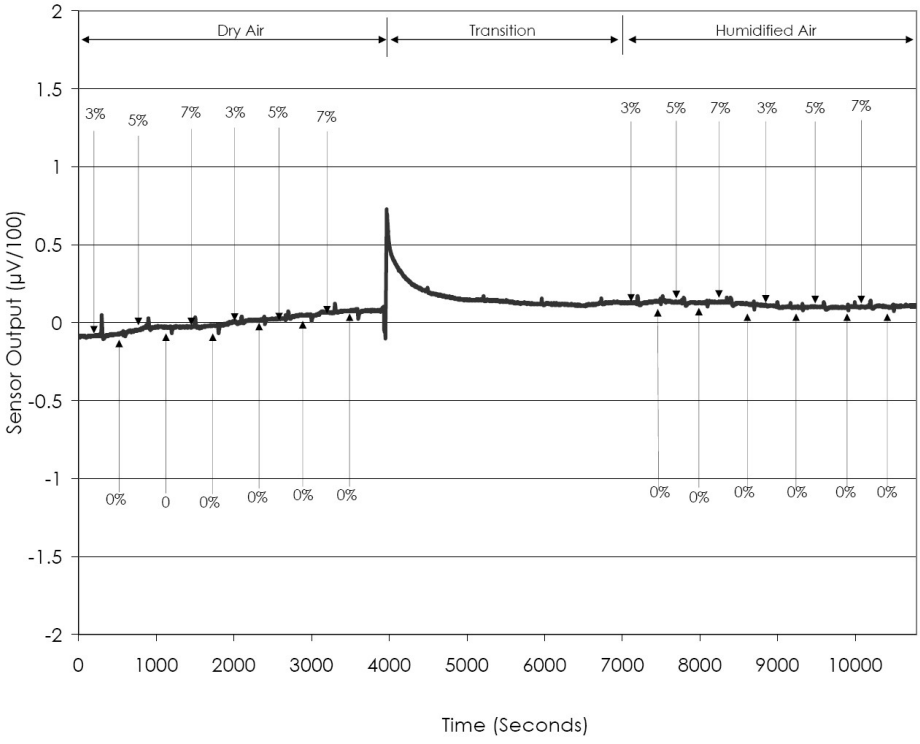

Figure 4.12: Polytetrafluoroethylene sensor output versus time with repeating changes in acetone exposure levels.

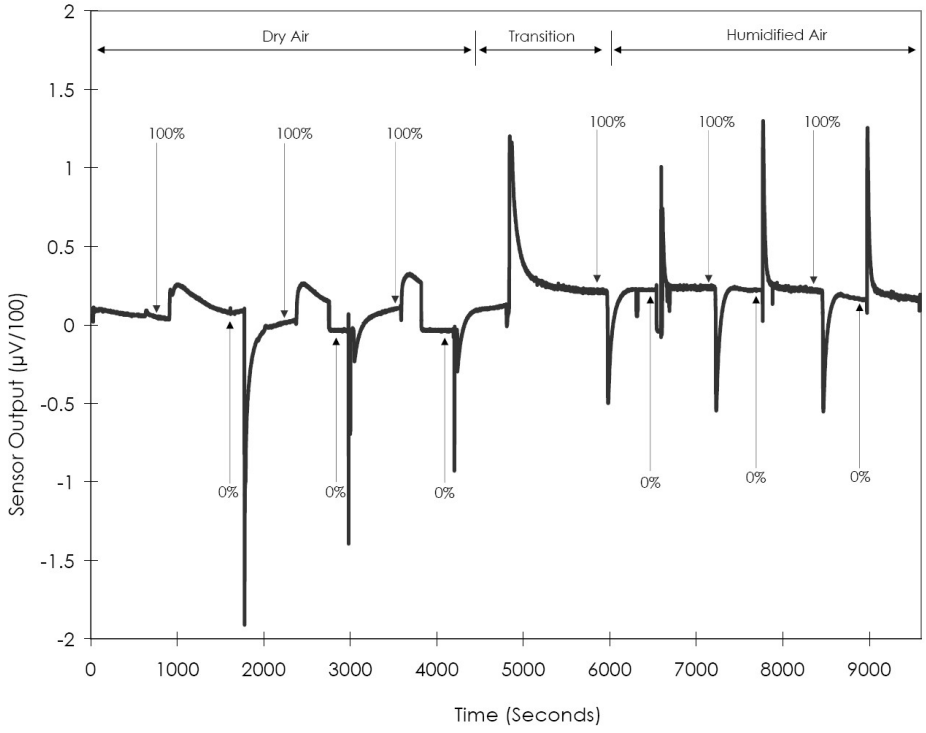

Figure 4.13: Polytetrafluoroethylene sensor output versus time with repeating changes in ethanol exposure levels.

Chapter 5

DISCUSSION

Transducer and Sensor Characterization

The value for 90% response time of the device was found to quite fast. Within one second, the device began to respond to incident light. Similar devices provided an average 90% response time of five seconds (Muehlbauer et al., 1990b). It is important to note that the recorded response time seemed longer than the visually observed response on the null meter that recorded device output. It is possible that increased sampling frequency might provide both enhanced resolution and perhaps an even smaller time constant for the device.

The baseline testing on the thermopile in acetone showed that the thermopile does not respond to acetone without the presence of a biorecognition element. This was an important first step in confirming that the thermopile and sensor design was recording analyte concentration without added noise.

The next step was to assess the repeatability of the device. The repeatability testing showed that the sensor with activated carbon as the biorecognition material was both repeatable and linear. The linear correlation coefficient value, R^2 was found to be 0.987. It was not possible to assess linearity with ethanol due to the test set up.

Biorecognition Material Evaluation

The activated charcoal experiments showed strong responses to both acetone and ethanol. The dry-air and humidified-air testing produced different results for both acetone and ethanol. For acetone the baseline value remained constant in dry air but shifted upward in humidified air. Additionally, the peak values for all acetone concentrations was lowered in humidified air. Similar results were seen

with ethanol. While the baseline value remained constant throughout dry and humidified air testing, the significant decrease in peak values was seen. A nearly 90% reduction in peak value was observed.

The interesting response for the activated charcoal with ethanol and humidified air suggests that an additional phenomenon occurred. Previous work has suggested that water may condense within the pores of activated charcoal (Delage et al., 1999). This could explain the endothermic response observed. However, the Delage findings were presented with acetone not ethanol. Additionally, the baseline shifting observed with acetone testing with activated charcoal seems to correlate with previous hysteresis findings observed when multiple adsorption desorption cycles are run in series (Gales et al., 2000).

The Dow Corning High Vacuum Stopcock Grease experiments showed an overall smaller response than the activated charcoal. However, there were similarities in the dry versus humidified air results. For instance, acetone testing in humidified air showed a upward baseline shift in acetone but not in ethanol. Different from charcoal, however, was that the peak values for all acetone concentrations remained constant in dry air and humidified air. Similar results were seen with ethanol. While the baseline value remained constant throughout dry and humidified air testing, there was no significant decrease in peak value. As with acetone, the peak values remained unchanged.

Polydimethylsiloxane performance was different from the other two materials. There was no baseline shift in the acetone testing from dry air to humidified air. Additionally, overall response to acetone diminished in the presence of humidity. Ethanol testing, on the other hand, experienced a baseline shift in a downward direction. This observation was accompanied by a decreased in the maximum peaks for ethanol as well.

Biorecognition Material	**Acetone Dry Air**	**Acetone Humidified Air**	**Ethanol Dry Air**	**Ethanol Humidified Air**
AC	$Peak_{max}$: 200 uV Distinct Curve No Baseline Shift	$Peak_{max}$: 200 uV Distinct Curve Baseline Shift Up	$Peak_{max}$: 25 uV Distinct Curve No Baseline Shift	$Peak_{max}$: -50 uV Distinct Curve No Baseline Shift
SCG	$Peak_{max}$: 100 uV Same Curve No Baseline Shift	$Peak_{max}$: 100 uV Same Curve Baseline Shift Up	$Peak_{max}$: 150 uV Same Curve No Baseline Shift	$Peak_{max}$: 150 uV Same Curve No Baseline Shift
PDMS	$Peak_{max}$: 125 uV Same Curve No Baseline Shift	$Peak_{max}$: 125 uV Same Curve No Baseline Shift	$Peak_{max}$: 150 uV Same Curve No Baseline Shift	$Peak_{max}$: 150 uV Same Curve Baseline Shift Down
PTFE	$Peak_{max}$: 1 uV Same Curve No Baseline Shift	$Peak_{max}$: 0.5 uV Same Curve No Baseline Shift	$Peak_{max}$: 175 uV Same Curve No Baseline Shift	$Peak_{max}$: 100 uV Same Curve No Baseline Shift

Table 5.1: Summary of data for both acetone and ethanol testing.

On the other hand, polytetrafluoroethylene, was by comparison, almost completely unresponsive to acetone. The baseline changes in the dry versus humidified air flow were negligible. This was also true for the ethanol testing. There was no significant baseline shift. There was however, a significant decrease in response to ethanol in humidified air. This response however was not symmetric, as it had been observed with the other three materials. Instead, the decrease was marginally seen in the endothermic desorption phase but markedly seen in exothermic portion of the desorption phase.

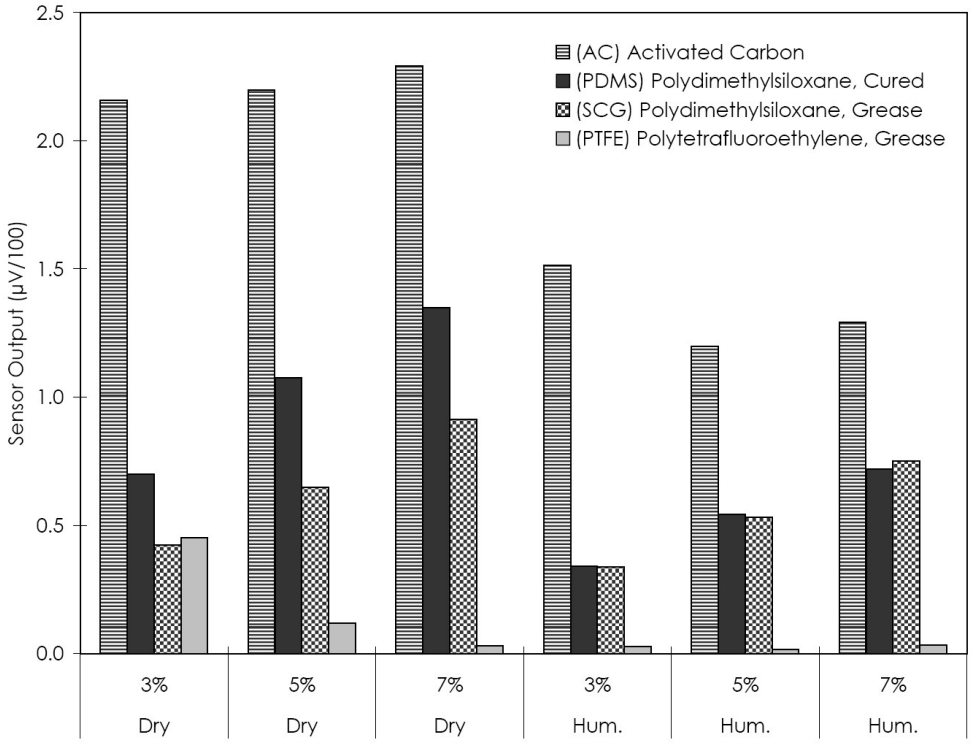

Figure 5.1: Peak output data for acetone testing with each biorecognition material.

The data presented in Figure 5.1 and 5.2 could be misleading. It is important to note that while the exposed surface are of the adsorbent remained constant throughout all testing, the depth of the biorecognition material was consistently maintained. Therefore, the direct comparison of each biorecognition material should be carefully considered.

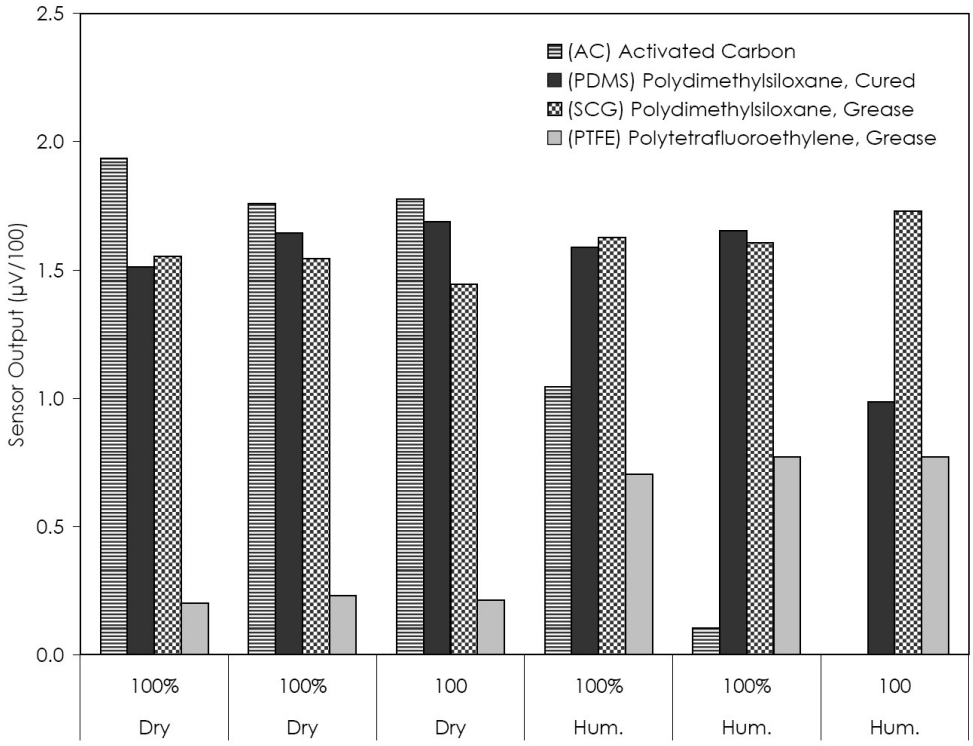

Figure 5.2: Peak output data for ethanol testing with each biorecognition material.

Evaluation of Theoretical Model

The evaluation of the thermoelectric model for the thermopile was reasonably successful. The sensitivity from the theoretical model, was most impacted by the absorbing material used, Kapton. In this case, the Kapton physical parameters were collected from the manufacturer. Additionally the device output was taken from the peak value of the real-time data shown in Figure 4.1. With this information, the sensitivity, was found to be 7.2 μV m^{o}C^{-1}, while the recorded value for this device from previous work was found to be 6.0 μV m^{o}C^{-1} (Guilbeau, 2008). The real device sensitivity would likely be reduced, since the heat capacity of the thermopile was assumed to be negligible.

To experimentally validate the the proposed energy balance for the thermoelectric heat of adsorption biosensor, literature values for the heats of adsorption

for activated charcoal could be used. At 40.0 kJ mol^{-1} and 41 kJ mol^{-1} for acetone and ethanol respectively the heats of adsorption provide a first step at evaluating the expected device output (Guo et al., 2011). The exposed surface area of the adsorbent would help approximate the moles of adsorbent adsorbed in a single monolayer. This information could then be compared to the output generated by a calibrated biosensor device. Suggestions for future work in this area are provided in the Conclusion and Recommendations section.

Chapter 6

CONCLUSIONS and RECOMMENDATIONS

In this work, a thermoelectric biosensor based upon adsorption chemistry was developed and characterized. The analytes, acetone and ethanol, were evaluated under dry air and humidified air conditions, and the sensor response to acetone concentration was found to be both repeatable and linear, while the sensor response to ethanol presence was also found to be repeatable. Further, the different biorecognition materials were found to produce discernible thermoelectric responses that were characteristic for each analyte. An overall assessment of the work done for this research effort is reviewed in the following section. Additionally, suggestions for further research are also presented.

From this work, it was determined that three of the four biorecognition materials could be used for both acetone and ethanol testing. Each material provided a significant response to both acetone and ethanol, and their responses were found to be repeatable. Further, humidity was found to have an impact on acetone and ethanol sensing. This dependence was subject to the material under evaluation.

One of the observations seen with respect to humidity was the baseline shifting during some humidified testing. It is possible that the peak output should have been processed to remove the observed shift. For instance, the raw data that was evaluated using Microsoft Excel software could have been processed for integration. Using MatLab Software, the area under the curve could have been used to remove the baseline data. This data analysis technique was successfully employed to analyze thermopile data used for thermoelectric sequencing of DNA (Nestorova and Guilbeau, 2011).

Further, to address the humidity concerns, it would be meaningful to correlate the humidity settings with average breath compositions. In this case, modifying the testing equipment to specify a physiological percent humidity in the flow stream would be useful. Also, conducting the experiments in a heated environment may yield good information for assessing the device in physiological conditions.

Regarding the test setup, modifications for further work would help yield more specific data. For instance, it would be useful to develop an apparatus for adding ethanol to the flow stream in variable quantified amounts. This information would allow for direct comparisons between acetone and ethanol results. Additionally, it would be useful to experimentally and theoretically define both limits of detection and clinical relevant values for the vaporizer settings. This would involve vaporizer modifications or upgrades.

Additionally, the complications that arise when a multicomponent system are evaluated should also be considered. Whether the interfering substances are water, organic compounds, or inorganic compounds, it is possible that an array of biosensors may be needed. Like previous multisensor array electric noses, that exploit solid-state sensor responses to specific gases (Paulsson and Winquist, 1999), the thermoelectric adsorption biosensor may need to have multiple sensors within one testing system. The processing algorithms for this type of device have been considered when the output of multiple sensors that specifically tests distant compounds are combined (Guo et al., 2011). This is certainly an exciting area for future work.

The model for the thermoelectric infrared detection device was found to be suitable. However, further development of the model for measuring heats of adsorption is needed. It would be useful to create complete individual isotherms for each biorecognition material and analyte. By appropriately plotting this isotherm

data, an experimental heat of adsorption could be compared to the device output. Additionally, given the multicomponent nature of the system, it maybe worthwhile to consider other isotherm models like the Temkin or Henderson isotherms.

Allison, S., Smith, R., Howard, D., Gonzlez, C., Collins, S., 2003. A bulk micromachined silicon thermopile with high sensitivity. Sensors and Actuators A: Physical 104 (1), 32–39.

Balzer, C., Wildhage, T., Braxmeier, S., Reichenauer, G., Olivier, J., 2011. Deformation of porous carbons upon adsorption. Langmuir 27 (6), 2553–2560.

Bataillard, P., Steffgen, E., Haemmerli, S., Manz, A., Widmer, H., 1993. An integrated silicon thermopile as biosensor for the thermal monitoring of glucose, urea and penicillin. Biosensors and Bioelectronics 8 (2), 89–98.

Caspary, D., Schrpfer, M., Lerchner, J., Wolf, G., 1999. A high resolution ic-calorimeter for the determination of heats of absorption onto thin coatings. Thermochimica Acta 337 (1-2), 19–26.

CDC, 2010. Obesity: halting the epidemic by making health easier. Tech. rep., Department of Health and Human Services, Centers for Disease Control and Prevention.

CDC, 2011. National diabetes fact sheet: national estimates and general information on diabetes and prediabetes in the united states. Tech. rep., Department of Health and Human Services, Centers for Disease Control and Prevention.

Charles, E., Groubert, E., Boyer, A., 1988. Thin-film thermopiles for measuring high laser powers. Sensors and Actuators 13 (2), 131–137.

Delage, F., Pr, P., Cloirec, P., 1999. Effects of moisture on warming of activated carbon bed. Journal of Environmental Engineering 125 (12), 1160–1167.

Domach, M., 2004. Introduction to biomedical engineering. Person Prince Hall, Upper Saddle River, NJ.

Dubowski, K., 1991. The technology of breath-alcohol analysis. Department of Health and Human Services, Rockville, MD.

Gales, L., Mendes, A., Costa, C., 2000. Hysteresis in the cyclic adsorption of acetone, ethanol and ethyl acetate on activated carbon. Carbon 38 (7), 1083–1088.

Graf, A., Arndt, M., Gerlach, G., 2007. Seebecks effect in micromachined thermopiles for infrared detection. a review. Estonian Journal of Engineering 13 (4), 338–353.

Guilbeau, E., 2008. Biosensor for measurement of breath acetone: Final progress report.

Guilbeau, E., Towe, B., Muehlbauer, M., 1987. A potentially implantable thermoelectric sensor for measurement of glucose. ASAIO Transactions 33 (3), 329–335.

Guo, D., Zhang, D., Zhang, L., 2011. An lda based sensor selection approach used in breath analysis system.

Herwaarden, A., Sarro, P., 1986. Thermal sensors based on the seebeck effect. Sensors and Actuators 10 (3-4), 321–346.

Lerchner, J., Caspary, D., Wolf, G., 2000. Calorimetric detection of volatile organic compounds. Sensors and Actuators B: Chemical 70 (1-3), 57–66.

Manohar, C., 2010. Are non-invasive techniques the future of medical device industry? HCL Technologies.

Miwa, Y., Tsutsumi, K., Takahashi, H., 1981. Measurement of heats of adsorption of carbon monoxide and carbon dioxide on cu(ii)-y zeolites by flow microcalorimetry. Zeolites 1 (2), 98–104.

Muehlbauer, M., Guilbeau, E., Towe, B., 1989. Model for a thermoelectric enzyme glucose sensor. Analytical Chemistry 61 (1), 77–83.

Muehlbauer, M., Guilbeau, E., Towe, B., 1990a. Applications and stability of a thermoelectric enzyme sensor. Sensors and Actuators B: Chemical 2 (3), 223–232.

Muehlbauer, M., Guilbeau, E., Towe, B., Brandon, T., 1990b. Thermoelectric enzyme sensor for measuring blood glucose. Biosensors and Bioelectronics 5 (1), 1–12.

Myers, A., 2002. Thermodynamics of adsorption in porous materials. AIChE Journal 48 (1), 145–160.

Myers, A., 2004. Thermodynamics of adsorption. In: Letcher, T. (Ed.), Chemical Thermodynamics for Industry. Royal Society of Chemistry, Cambridge, UK.

Myers, A., Siperstein, F., 2001. Characterization of adsorbents by energy profile of adsorbed molecules. Colloids and Surfaces A: Physicochemical and Engineering Aspects 187-188, 73–81.

Nestorova, G., Guilbeau, E., 2011. Thermoelectric method for sequencing dna. 1473-0197.

Pan, H., Ritter, J., Balbuena, P., 1998. Examination of the approximations used in determining the isosteric heat of adsorption from the clausiusclapeyron equation. Langmuir 14 (21), 6323–6327.

Paulsson, N., Winquist, F., 1999. Analysis of breath alcohol with a multisensor array: instrumental setup, characterization and evaluation. Forensic Science International 105 (2), 95–114.

Pizziconi, V., Page, D., 1997. A cell-based immunobiosensor with engineered molecular recognition–part i: design feasibility. Biosensors and Bioelectronics 12 (4), 287–299.

Room, R., Babor, T., Rehm, J., 2005. Alcohol and public health. The Lancet 365 (9458), 519–530.

Sharma, P., Singh, D., 2011. Adsorption. http://www.xamplified.com. Xamplified, New Delhi, India.

Towe, B., Guilbeau, E., 1996. A vibrating probe thermal biochemical sensor. Biosensors and Bioelectronics 11 (3), 247–252.

Weckmann, S., 1997. Dynamic electrothermal model of a sputtered thermopile thermal radiation detector for earth radiation budget applications. Ph.D. thesis, Virginia Polytechnic Institute and State University.

Xie, B., Mecklenburg, M., Danielsson, B., hman, O., Winquist, F., 1994. Microbiosensor based on an integrated thermopile. Analytica Chimica Acta 299 (2), 165–170.

Xue, C., Wang, K., Liang, T., Zhang, W., Xiong, J., 2010. Ir characterization of carbon-black for thermopile infrared detectors. In: Nano/Micro Engineered and Molecular Systems (NEMS), 2010 5th IEEE International Conference on. pp. 963–966.

APPENDIX

The work presented below shows sample calculations used to asses the thermo-electric model of the infrared detector. The sample calculations were produced using Mathcad Software.

Characterizing the Incident Radiant Energy

$power := 5mW$ generated by a laser pen

Determining the Total Junction Area

$njunction := 58$

$junction\_area := 0.2mm^2$

Characterizing the Absorbing Layer

$k\_kapton := 0.12\frac{W}{m \cdot K}$ coefficient of thermal conductivity for Kapton

$depth\_kapton := 75 \times 10^{-6} m$

$conductance := k\_kapton \cdot \frac{njunction \cdot junction\_area}{depth\_kapton}$ conductance for Kapton

$conductance = 0.019\frac{W}{K}$

$heatabsorbed := \frac{power}{conductance}$

$heatabsorbed = 0.269K$

Experimentally Determined Thermopile Output

$output := 1.95mV$

Characterizing Thermopile Sensitivity

$sensitivity := \frac{output}{heatabsorbed}$

$sensitivity = 7.238 \times 10^{-3}\frac{V}{\Delta°C}$

BIOGRAPHICAL SKETCH

Kimberly Joree Wilson received her undergraduate degree in Chemical Engineering from Carnegie Mellon University in Pittsburgh, PA. As a Product Development Engineer, Kimberly applied her chemical engineering skills to the semiconductor industry before returning to academic studies. She then completed a graduate degree in Bioengineering at Arizona State University in Tempe, AZ. Kimberly will further her interests in the biomedical sciences as a medical student. Her goal is to become a phenomenal, practicing physician.